Hindawi
Journal of Engineering
Volume 2024, Article ID 5590437, 31 pages
https://doi.org/10.1155/2024/5590437

Research Article

CFD Simulation of an Industrial Dust Cyclone Separator: A Comparison with Empirical Models: The Influence of the Inlet Velocity and the Particle Size on Performance Factors in Situation of High Concentration of Particles

Tchinda Vermande Paganel,[1] **Epee Fabrice Alban**,[1,2] **Mezoue Adiang Cyrille**,[1,2] **and Claude Valery Ngayihi Abbe**[1,2,3]

[1]*Laboratory of Energy, Materials, Modeling, and Methods, Higher National Polytechnic School of Douala, University of Douala, P.O Box 2701, Douala, Cameroon*
[2]*Higher National Polytechnic School of Douala, University of Douala, P.O. Box 2701, Douala, Cameroon*
[3]*Department of Mechanic Engineering, Higher National Polytechnic School of Douala, University of Douala, P.O. Box 2107, Douala, Cameroon*

Correspondence should be addressed to Tchinda Vermande Paganel; paganeltchinda@gmail.com

Received 5 July 2023; Revised 23 December 2023; Accepted 19 February 2024; Published 14 March 2024

Academic Editor: Oronzio Manca

The present work is dedicated to the study of multiphase turbulent and three-dimensional rotational flow in dust cyclones, a contribution to air pollution control. Cyclones are widely used devices for the separation of constituents from solid-gas mixtures in industry. In order to improve the filtration efficiency of cyclones, and to reduce the pressure drop, parametric numerical simulation studies using the Fluent code have been conducted to characterise the effects of the parameters affecting the operation of these devices through their performance indicators. In this work, the effect of inlet velocity and the particle size on the turbulent flow air in the cyclone is presented. Numerical simulation of the flow by Fluent code using three numerical models: the first based on the dissipation of kinetic energy by viscosity (RNG) K-epsilon and standard K-epsilon as well as the last based on the solution of Reynolds stress equations (RSM), combined with the multiphase mixing model, gave interesting results in terms of the pressure and flow field in the separator, the variation of inlet velocity, and the variation of particle size. Validation with experimental and empirical results showed the advantage of the Reynolds stress turbulence model (RSM) over the standard K-epsilon and RNG K-epsilon. The RSM model better captures physical phenomena in an intense vortex flow in the presence of walls. But it is characterised by a very long calculation time and requires large machine resources. An alternative to this model is RNG K-epsilon model, which offers a reasonable calculation time with acceptable results (maximum deviation of 5 %) for speed values below 10 m/s. In the absence of numerical resources, certain empirical models such as those of First (for the evaluation of pressure drop) and Iozia and Leith (for evaluation of efficiency) may well be useful for the dimensioning of the cyclone.

1. Introduction

The industry is currently subject to environmental and hygiene requirements (international regulations limit the dust content of workplaces to 5 mg/m^3 of air for respirable dust) [1]. It turns out that cyclones do a good job of removing dust from exhaust gas. In addition, they can satisfy the need to separate the components of a mixture for individual component operation [2–6]. These advantages have enabled this technique to be extended to a number of industrial fields, including the food industry, the hydrocarbon industry, the cement industry, the mechanical industry, foundry (air filtration, iron trapping, etc.), the waste treatment industry, soil decontamination, combustion (burner and combustion chamber), heat exchangers, the biomass, and biotechnology [2, 4, 7, 8].

The proper definition of the work of a cyclone is defined by the product of the centrifugal forces acting on the particles suspended in an air stream [4, 7]. As the particles have a higher density than the gas, they are forced toward the wall of the cyclone, where, once deposited, they are transported down the cone, to the outlet where they are collected [4, 9]. The clean gas, now free of some of its dust load, rises through the center of the cyclone, escaping through the outlet tube, which passes through the roof [10]. Imagine that the gas enters through the inlet at the top of the cyclone (tangentially), then spirals downward (first vortex) until it reaches the point where the diameter of the cone is equal to the diameter of the outlet in the roof (vortex finder) (Figure 1). Finally, the gas rises through the center, creating a second vortex in the opposite direction to the first, and then escapes through the hole through the roof [4, 9, 11, 12].

The cyclone separator, which has many advantages such as simple structure, high separation efficiency, low energy consumption, and easy operation, has been widely used in engineering processes to separate dispersed solid particles from suspension by centrifugal and vortex action [4]. However, the common cyclone shows a low efficiency for fine particles [13]. Many attempts have been conducted to improve the separation performance of cyclone separators by optimizing the structure dimension, such as vortex length [14, 15], vortex finder shape and diameter [16–18], inlet type, including single, double inlet and more than two inlets [19–21], tangential, and spiral inlet [20], inlet dimension [22], different inlet section angles in relation to the cyclone body [23–25], symmetrical inlet and a volute scroll outlet [26], cone tip diameter [27, 28], cyclone height [29], conical length [18, 30, 31], diameter and length of vortex finder [32, 33] and hopper length [9]. There are also various kinds of cyclone separators developed to improve the separation efficiency, such as Lee type [34], semi-spherical cyclone [35], dynamic cyclone [36], square cyclone [37], CFC cyclone [38], and the new generation of cyclone separators presented as multichannel cyclone separators [39–43]. The multichannel cyclone separator's structure has some essential external and internal elements, including upgraded curved elements with openings cut with their plates bent outwards to make curvilinear channels for the continuous movement of the peripheral and transitional gas flows from the inflow opening to the central axis [39]. In contrast to the study of the conventional cyclone separator, where the modeling is studied in particular detail, the operating principle and design of this new generation equipment is not well understood [39, 43]. However, although the improvements have been observed, these techniques cannot significantly improve the collection efficiency for microsized particles. In the word, many attempts have been conducted to improve the separating capacity of fine particles from the exhaust gas. However, the design of a high efficiency, low-energy consumption, and low-maintenance separation system with a simple structure for fine particle is still a challenge.

The study of cyclones is motivated by their use in many industrial sectors (mentioned above) because of the multiple advantages they offer, notably their simplicity, compactness (10% of the surface can be occupied by other industrial equipment) [3, 11, 44–46], low manufacturing and maintenance costs, very short residence time (1 to 2 seconds), insensitivity to orientation due to the intense rotational field (of the order of thousands of times the gravitational field), and the absence of moving parts [4, 47].

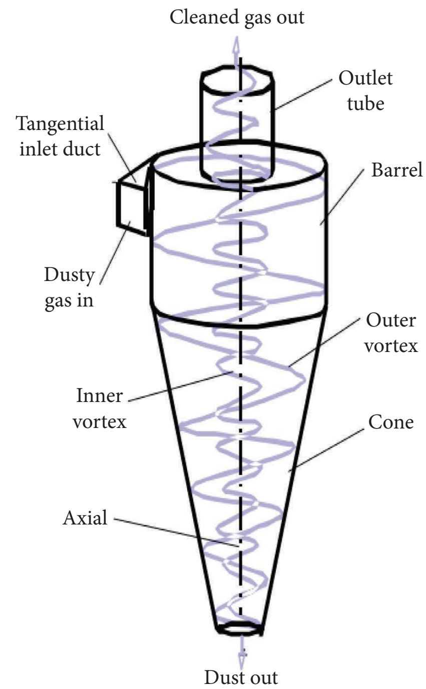

Figure 1: Vortex phenomenon inside a cyclone separator [9]. (This figure is reproduced from Lingjuan Wang 2004 (under the Creative Commons Attribution License/public domain)).

However, the flow within these devices is very complex. The flow is highly turbulent with a three-dimensional, sometimes unsteady behavior. This complexity is compounded by the presence of several phases with different characteristics and trajectories [2, 9].

During the past decades, experimental studies have shown their limitations, especially in the measurement of the parameters affecting the performance factors, due to the complexity of the cyclone geometry (its closed space) [2].

Numerical studies, in particular CFD, appear to be the best means of studying and analysing the indicators (velocity fields, pressure fields, and temperature fields) that affect the performance factors (efficiency and pressure drop) [9, 48, 49]. Among the most widely used codes, the FLUENT code is the most widely used code in the CFD analysis of cyclone separators.

The main objective of this work is the treatment by numerical simulation of the turbulent three-dimensional flow of a Newtonian incompressible two-phase fluid (gaseous and solid phase) in a cyclone dust separator. The CFD will be preceded by a theoretical evaluation which will include the choice of the type of cyclone (type of entry), the calculation of its dimensions, the analysis of empirical models of comparison and the choice of numerical simulation models.

An analysis will be made on different fields (velocity and pressure) influencing the efficiency of the separator. The influence of inlet velocity and particle size in the gas phase will be the main factors of comparison.

1.1. Cyclone Separator Geometry. The cyclone model chosen for the numerical calculation is the Stairmand model [8, 49–51]. It is a cyclone with single tangential inlet. The geometry is given in Figure 2 and the ratios of dimensions with respect to D are presented in Table 1. We have chosen an industrial application cyclone with a body diameter of $D = 300$ mm, with a cone base diameter extension and discharge hopper [9].

2. Numerical Simulation

2.1. Numerical Procedure

2.1.1. Computation of the Grid. The study of the mesh is essential in the numerical simulation, as the accuracy of the solution depends on the grid used (Figure 3). Geometry and the mesh have been developed in Fluent. We have chosen a tetrahedral mesh as shown in Figure 3 with 134 642 elements; 25 125 nodes. The simulation with a tetrahedral mesh gives good results for the case of a cyclone, according to Slack [52]. The mesh can be suitably refined in Fluent to properly control the results.

2.1.2. Solver. The numerical simulation of the fluid flow in the cyclone separator having complex geometry and a closed space was performed with the solver FLUENT, version R19.2. FLUENT is a coupled implicit numerical solver, which incorporates finite volume methods to discretise the equations that govern fluid dynamics in a spatial domain [53]. The simulations were conducted on an HP computer with an INTEL(R) Core i3-4005U CPU@1.70 GHz; a 8 GHz RAM memory; and a 64 bit operating system.

2.1.3. Boundary Conditions. Boundary conditions, in this case, surface conditions, are conditions that completely define the flow characteristics in the cyclone separator. These surfaces here are the "inlet" (Figure 4(a)) or entry surface which is the section at which the exhaust gas enters the separator; the "outlet" (Figure 4(b)) or exit section which is the face through which the clean gases escape with the finest particles, the collection or "Collection bin" (Figure 4(c)) which represents the collection section of the particles of the solid phase of the mixture; the "WALL" which represents the body of the separator. The temperature of the gas (air with density $\rho_g = 1.225\,\mathrm{kg/m^3}$) used as the continuous phase for the general study was fixed at 300 K, and the steel particles (sizes : $5\mu_m$; density: $8030\,\mathrm{kg/m^3}$) as the solid transport particles (dispersed phase).We assumed spherical particles with a loading of $C_o = 500g$ dust per m^3 of air (sectors such as metal refining, blast furnaces, the iron and steel industry, metal machining, etc.). Atmospheric pressure was used as the reference pressure.

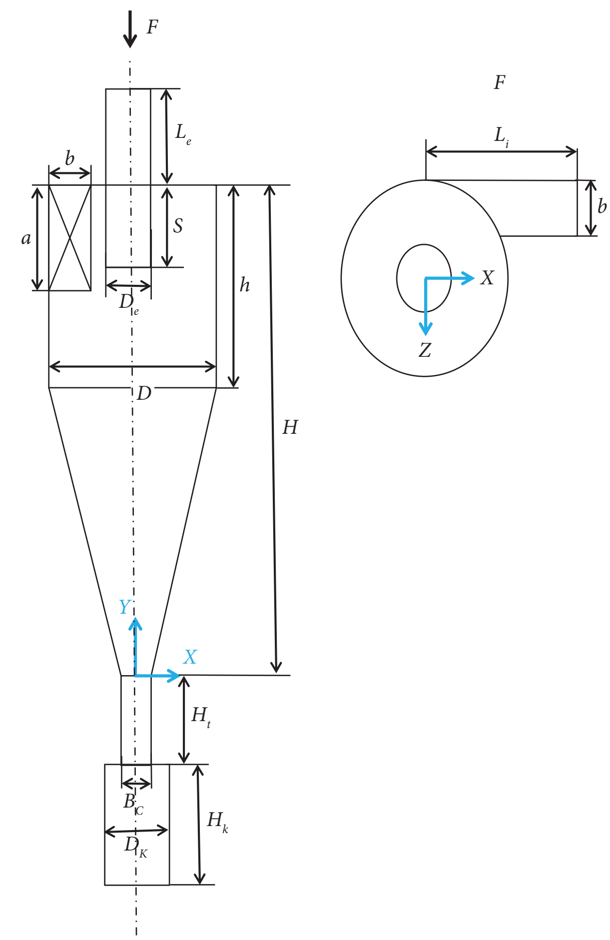

Figure 2: 2D geometry of the cyclone.

Table 1: Geometrical parameters of the cyclone dust separator.

Parameters	Ratio dimension/D
Body diameter **D**	1
Inlet tube length **a**	0.5
Inlet tube width **b**	0.5
Vortex finder diameter $\mathbf{D_e}$	0.2
Vortex finder height **S**	0.5
Cone base diameter $\mathbf{B_c}$	0.375
Cyclone height **H**	4
Body height **h**	1.5
External extension of the vortex finder $\mathbf{L_e}$	0.666
Extension of the inlet $\mathbf{L_i}$	0.666
Cone tip length $\mathbf{H_t}$	0.5
Collector height $\mathbf{H_k}$	1
Collector diameter $\mathbf{D_k}$	0.666

2.1.4. Fluid Flow Modeling. We know in advance that the flow behavior is turbulent in nature in most (or all) industrial cyclones. Turbulent flow is described by the Navier-Stokes equations. But in a general framework, it is impossible to solve these equations directly [53]. The Navier-Stokes equations can be put in tensor form as follows [46, 54]:

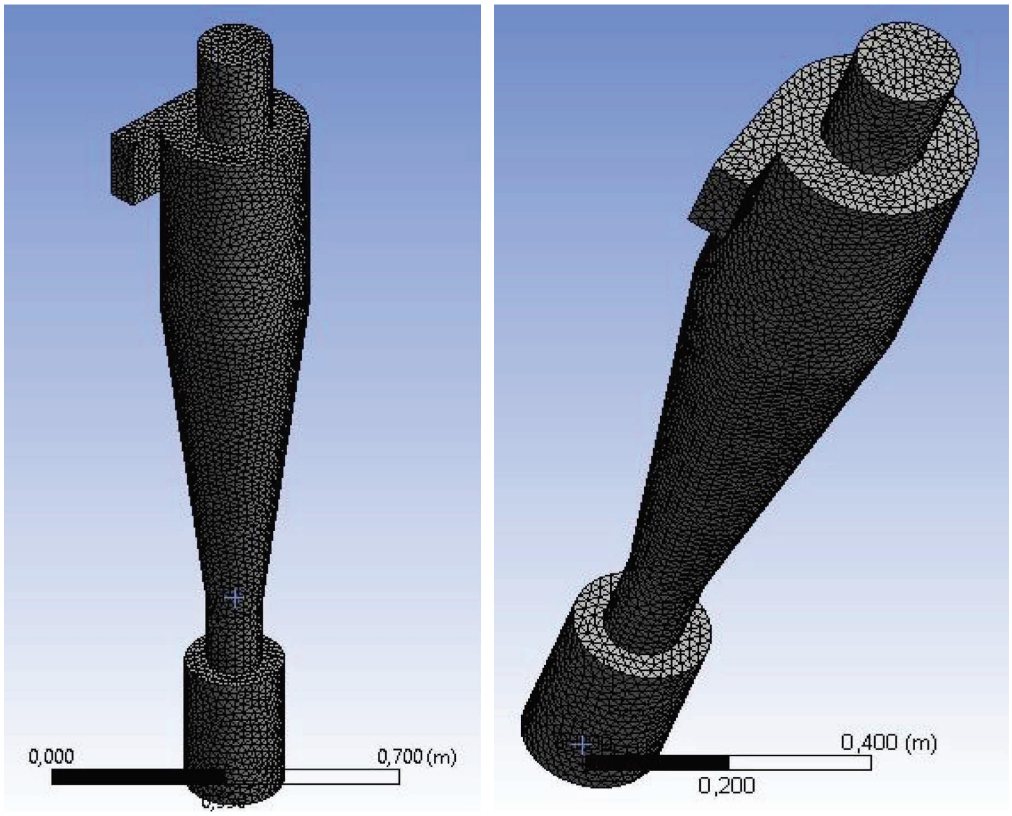

Figure 3: The mesh.

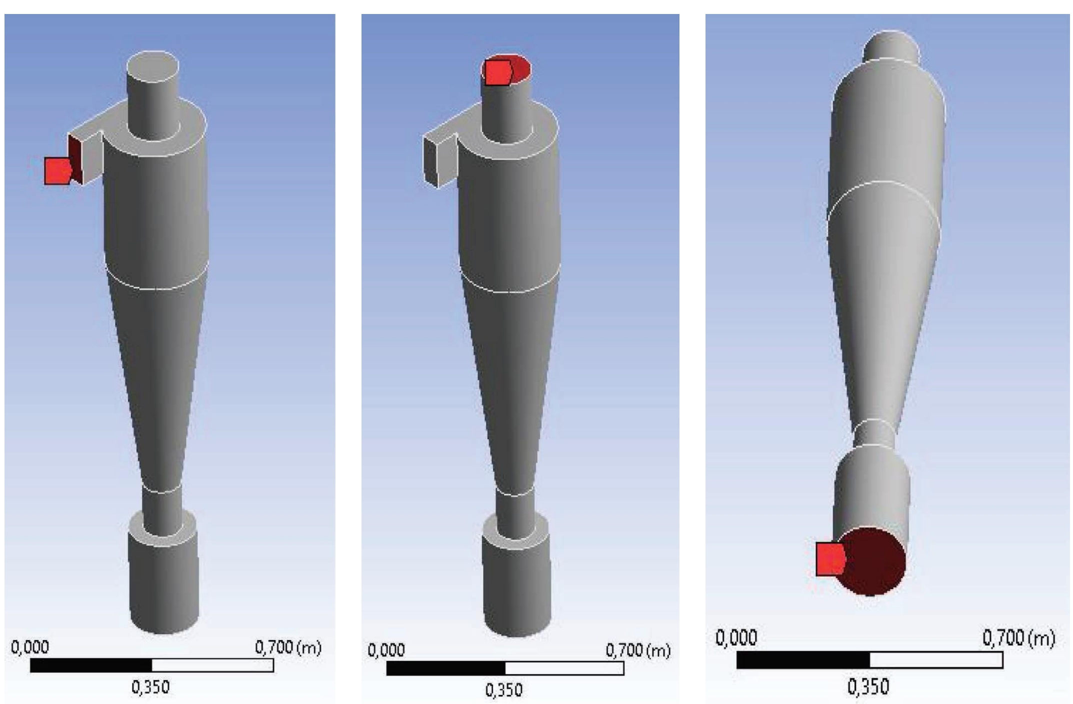

(a) (b) (c)

Figure 4: Boundary conditions.

$$\begin{cases} \dfrac{\partial \rho}{\partial t} - \dfrac{\partial (\rho u_i)}{\partial x_i} = 0, \\ \dfrac{\partial \left(\rho u_j\right)}{\partial t} + \dfrac{\partial \left(\rho u_i u_j\right)}{\partial x_i} = \dfrac{\partial}{\partial x_i}\left(\tau_{ij}^l - P\delta_{ij}\right), \\ \dfrac{\partial (\rho E)}{\partial t} + \dfrac{\partial (\rho u_i E)}{\partial x_i} = \dfrac{\partial}{\partial x_i}\left(\tau_{ij}^l u_j - P\delta_{ij} u_j - Q_j\right). \end{cases} \tag{1}$$

In this study, we used three numerical simulation models to solve the fluid flow problem of the cyclone.

(1) Reynolds Stress Models (RSM). This model was used to analyse the behavior of the different parameters that affect the pressure drop and the efficiency of the separator, namely: the velocity field and the pressure field. The RSM model presents the best behavior of the fluid in the separator [9, 33]; it predicts well the two vortices as well as the fluid flow field in the separator, and finally the tangential velocity [46, 55]. The form of the final equation is

$$\begin{aligned} \frac{\partial\left(\overline{\rho}\widetilde{u_i''u_j''}\right)}{\partial t} + \frac{\partial\left(\widetilde{u}_j\overline{\rho}\widetilde{u_i''u_j''}\right)}{\partial x_k} &= -\left(\overline{\rho}\widetilde{u_j''u_k''}\frac{\partial \widetilde{u}_i}{\partial x_k} + \overline{\rho}\widetilde{u_i''u_k''}\frac{\partial \widetilde{u}_j}{\partial x_k}\right) \\ &\quad - \frac{\partial}{\partial x_k}\left[\overline{\rho}\widetilde{u_i''u_k''u_j''} + \overline{P'u_j''}\delta_{ik} + \overline{P'u_i''}\delta_{jk} - \left(\overline{\mu S_{ik} u_j''} + \overline{\mu S_{jk} u_i''}\right)\right] \\ &\quad + \overline{P'\left(\frac{\partial u_i''}{\partial x_j} + \frac{\partial u_j''}{\partial x_i}\right)} - \left(\overline{\mu S_{ik}\frac{\partial u_k''}{\partial x_k}} + \overline{\mu S_{jk}\frac{\partial u_k''}{\partial x_k}}\right) - \overline{u_j''}\frac{\partial \overline{P}}{\partial x_i} - \overline{u_i''}\frac{\partial \overline{P}}{\partial x_j}. \end{aligned} \tag{2}$$

The numerical discretisation scheme for general study case with The RSM model is presented in Table 2, and Boundary conditions in Table 3.

(2) The Standard k-Epsilon Model. The numerical turbulence model used for the analysis of the effect of inlet velocity on pressure drop and separator efficiency is the standard k-epsilon ($k-\varepsilon$) turbulence model; because, it not only allows flows to be modeled with fully turbulent flow [57], but also assumes that the fluid has the same physical properties in all directions. The Navier-Stokes system coupled to the *k*-epsilon model is written as [54]

$$\begin{cases} \dfrac{\partial \overline{\rho}}{\partial t} - \dfrac{\partial (\overline{\rho}\widetilde{u}_i)}{\partial x_i} = 0, \\ \dfrac{\partial (\overline{\rho}\widetilde{u}_i)}{\partial x_i} + \dfrac{\partial}{\partial x_i}\left(\overline{\rho}\widetilde{u}_i\widetilde{u}_j + \overline{P}\delta_{ij}\right) = \dfrac{\partial}{\partial x_i}\left[(\overline{\mu} + \mu_t)\widetilde{S}_{ij} - \dfrac{2}{3}\overline{\rho}\widetilde{k}\delta_{ij}\right], \\ \dfrac{\partial (\overline{\rho}\widetilde{E})}{\partial t} + \dfrac{\partial \widetilde{u}_i(\overline{\rho}\widetilde{E} + \overline{P})}{\partial x_i} = \dfrac{\partial}{\partial x_i}\left[(\overline{\mu} + \mu_t)\widetilde{S}_{ij}\overline{u_j''} + \left(\overline{\lambda} + \lambda_t\right)\dfrac{\partial \widetilde{T}}{\partial x_i} + \dfrac{\mu_t}{\sigma_k}\dfrac{\partial \widetilde{k}}{\partial x_i} - \dfrac{2}{3}\overline{\rho}\widetilde{k}\delta_{ij}\right], \\ \dfrac{\partial (\overline{\rho}\widetilde{k})}{\partial t} + \dfrac{\partial\left(\widetilde{u}_i\overline{\rho}\widetilde{k}\right)}{\partial x_i} = \dfrac{\partial}{\partial x_i}\left[\left(\overline{\mu} + \dfrac{\mu_t}{\sigma_k}\right)\dfrac{\partial \widetilde{k}}{\partial x_i}\right] + \mathscr{P} - \overline{\rho\varepsilon}, \\ \dfrac{\partial (\overline{\rho\varepsilon})}{\partial t} + \dfrac{\partial (\widetilde{u}_i\overline{\rho\varepsilon})}{\partial x_i} = \dfrac{\partial}{\partial x_i}\left[\left(\overline{\mu} + \dfrac{\mu_t}{\sigma_\varepsilon}\right)\dfrac{\partial \overline{\varepsilon}}{\partial x_i}\right] + C_{\varepsilon 1}\dfrac{\widetilde{\varepsilon}}{\widetilde{k}}\mathscr{P} - C_{\varepsilon 2}\dfrac{\widetilde{\varepsilon}^2}{\widetilde{k}}\overline{\rho\varepsilon} + \text{Comp}, \end{cases} \tag{3}$$

with $\mu_t = C_\mu \rho k^2/\varepsilon$, $C_\mu = 0.09$, $C_{\varepsilon 1} = 1.44$, $C_{\varepsilon 2} = 1.92$, $\sigma_k = 1.0$, et $\sigma_\varepsilon = 1.30$.

The numerical discretisation scheme for general study case with the standard k-epsilon model is presented in Table 4, and Boundary conditions in Table 5.

(3) The RNG $k-\varepsilon$ Model. The numerical turbulence model used for the analysis of the effect of particle size on the efficiency of the separator is the RNG *k*-epsilon ($k-\varepsilon$) turbulence model, as this closure model takes into account vortex effects in the turbulence and the velocity of the forced

Table 2: Discretisation scheme for general study case [56].

Pressure-velocity coupling	
Scheme	Simple
Spatial discretisation	
Gradient	Least squares cell based
Pressure	Second order
Momentum	Second order upwind
Turbulent kinetic energy	Second order upwind
Turbulent dissipation rate	Second order upwind
Reynolds stress	Second order upwind
Energy	Second order upwind

Table 3: Boundary conditions for study general study case.

Inlet	
Model	Reynolds stress model (RSM)
Inlet velocity	10 m/s
Intensity of turbulence	5%
Hydraulic diameter	0.0857 m
Temperature	300 K
DPM	Reflect
Outlet	
DPM	Escape
Hydraulic diameter	0.15 m
Collection bin	
DPM	Trap
Wall	
DPM	Reflect

Table 4: Discretisation scheme for study the effect of inlet velocity [56].

Pressure-velocity coupling	
Scheme	Simple
Spatial discretisation	
Gradient	Least squares cell based
Pressure	Second order
Momentum	Second order upwind
Turbulent kinetic energy	Second order upwind
Turbulent dissipation rate	Second order upwind

Table 5: Boundary conditions for study the effect of inlet velocity.

Inlet	
Model	$k-\boldsymbol{\varepsilon}$ standard
Inlet velocity	$V_{i(\text{int})}$ (m/s), $i = 1\ldots10$
Intensity of turbulence	5%
Hydraulic diameter	0.0857 m
Temperature	300 K
DPM	Reflect
Outlet	
DPM	Escape
Hydraulic diameter	0.15 m
Collection bin	
DPM	Trap
Wall	
DPM	Reflect

flow, but also has the ability to be used to resolve low Reynolds number flow effects in the vicinity of boundary layer walls [2, 58].

$$\begin{cases} \dfrac{\partial(\overline{\rho}\widetilde{k})}{\partial t} + \dfrac{\partial\left(\widetilde{u}_i\overline{\rho}\widetilde{k}\right)}{\partial x_i} = \dfrac{\partial}{\partial x_i}\left[\alpha_k\mu_{\text{eff}}\dfrac{\partial\widetilde{k}}{\partial x_i}\right] + G_k + G_b - \overline{\rho\varepsilon} - Y_m + S_k, \\ \dfrac{\partial(\overline{\rho\varepsilon})}{\partial t} + \dfrac{\partial(\widetilde{u}_i\overline{\rho\varepsilon})}{\partial x_i} = \dfrac{\partial}{\partial x_i}\left[\alpha_\varepsilon\mu_{\text{eff}}\dfrac{\partial\widetilde{\varepsilon}}{\partial x_i}\right] + C_{\varepsilon1}\dfrac{\widetilde{\varepsilon}}{\widetilde{k}}(G_k + C_{3\varepsilon}G_b) - C_{\varepsilon2}\dfrac{\widetilde{\varepsilon}^2}{\widetilde{k}}\overline{\rho\varepsilon} - R_\varepsilon + S_\varepsilon. \end{cases} \tag{4}$$

where α_k and α_ε are inverses of the effective Prandtl numbers for the kinetic energy k and the mean dissipation $\widetilde{\varepsilon}$, respectively. The normalisation group term for the dissipation ε is

$$R_\varepsilon = \frac{C_\mu\rho\eta^3\left(1-(\eta/\eta_0)\right)}{1+\beta\eta^3}\frac{\varepsilon^2}{k}, \tag{5}$$

where $\approx$Sk/ε ; $\eta_0 = 4.38$; et $\beta = 0.012$.

G_k represents the generation of turbulence kinetic energy due to velocity variation; G_b represents the generation of turbulence kinetic energy due to buoyancy; Y_m represents the contribution of the fluctuating expansion of compressible turbulence to the overall dissipation rate; S_k et S_ε represent the source terms; $C_{\varepsilon1}$, $C_{\varepsilon2}$, and $C_{\varepsilon1}$ are constants.

The numerical discretisation scheme for general study case with the RNG k-epsilon model is presented in Table 6, and Boundary conditions in Table 7.

(4) Equations Governing the Solid Phase. The equations of motion of the particles with the Euler–Lagrange approach are given by [3, 48, 49]:

$$\begin{cases} \dfrac{du_{\text{pi}}}{dt} = F_d\left(u_i - u_{pi}\right) + g_i\dfrac{\left(\rho_p-\rho\right)}{\rho_p} + F_x, \\ \dfrac{dx_{pi}}{dt} = u_{pi};\ i = 1,\ 2,\ 3, \end{cases} \tag{6}$$

Table 6: Discretisation scheme for study the effect of particle size [56].

Pressure-velocity coupling	
Scheme	Simple
Spatial discretisation	
Gradient	Least squares cell based
Pressure	Second order
Momentum	Second order upwind
Turbulent kinetic energy	Second order upwind
Turbulent dissipation rate	Second order upwind

Table 7: Boundary conditions for the study the effect of particle size.

Inlet	
Model	**RNG** $k-\varepsilon$
Inlet velocity	$V_{i(\text{int})}$ $(m/s), i = 1 \ldots 3$
Intensity of turbulence	5%
Hydraulic diameter	0.0857 m
Temperature	300 K
DPM	Reflect
Outlet	
DPM	Escape
Hydraulic diameter	0.15 m
Collection bin	
DPM	Trap
Wall	
DPM	Reflect

where x_{pi} is the *ith* coordinate of the particle; g_i is the acceleration of gravity in i direction; ρ_p and ρ are the densities of the particle and the gas, respectively.

Generally, the difference between the particles velocity and the fluid velocity result from the imbalance of the pressure distribution and the viscous tensions on the particle surfaces. This gives rise to the drag force forces F_d which can be calculated by

$$F_d = \frac{1}{\tau_P}\frac{C_d R_{\text{ep}}}{24}, \tag{7}$$

where τ_P, the relaxation time of the particle is given by

$$\tau_P = \frac{\rho_p d_p^2}{18\mu}. \tag{8}$$

The drag coefficient C_d is a function of the particle Reynolds number defined by

$$R_{\text{epi}} = \rho d_p \frac{\left|u_i - u_{\text{pi}}\right|}{\mu}. \tag{9}$$

Morsi and Alexander [59] define the drag coefficient for spherical particles as

$$C_d = \begin{cases} \dfrac{24}{R_{ep}} & R_{ep} \le 1, \\ \dfrac{24\left[1 + 0.15\left(R_{\text{ep}}\right)^{0.687}\right]}{R_{ep}} & 1 < R_{\text{ep}} \le 1000, \\ 0.44 & 1000 < R_{\text{ep}}. \end{cases} \tag{10}$$

F_x is the additional acceleration (force per unit mass of particle); it was defined by Saffman [3] as

$$F_x = \frac{2K\sqrt{u_i}\,\rho_p d_{\text{ij}}}{\rho_p d_p \left(\rho_{\text{kl}} d_{\text{kl}}\right)^{0.25}}\left(u_i - u_{\text{pi}}\right), \tag{11}$$

where d_{ij} is the deformation tensor and $K = 2.594$.

2.1.5. Centrifugal Force. Centrifugal force plays an important role in the separation of particles. Centrifugal force is usually presented as a pseudoforce that arises directly from the transport of the inertia of a body when another force sets it in motion in a curved region. If the particle moves in a curved region with a radius r and velocity V_c along the region, then it has angular velocity:

$$\omega = \frac{V_c}{r}. \tag{12}$$

And the centrifugal force

$$\begin{aligned} F_c &= \frac{mV_c^{\,2}}{r} \\ &= m\omega^2 r. \end{aligned} \tag{13}$$

For cyclone analysis, the centrifugal force is commonly expressed as its ratio to the force of gravity [47]:

$$\begin{aligned} \frac{\text{centrifugal } \textit{Force}}{\text{force of gravity}} &= \frac{F_c}{F_g} \\ &= \frac{\left(mV_c^{\,2}/r\right)}{\text{mg}} \\ &= \frac{V_c^{\,2}}{\text{rg}}. \end{aligned} \tag{14}$$

2.1.6. Numerical Inlet Data of Studies

(i) To analyse the influence of inlet velocity on performance factors, we based our analysis in the literature [50] on the experimental work of Stairmand (1969); Swift (1969); and Lapple (1951) (Table 8), who determined the ratio of flow rate to cyclone cylinder

Table 8: Inlet velocities.

Source	Stairmand (1951)	Swift (1969)	Lapple (1951)	Swift (1969)	Swift (1969)	Stairmand (1951)
Recommended duty	High efficiency	High efficiency	General purpose	General purpose	High throughput	High throughput
Q/D (m/hr)	5 500	4 940	6 860	6 680	12 500	16 500
$V\ (m/s)$	13.72	15.27	18.55	19.05	37.72	45.83

diameter. These values enabled us to determine the different inlet velocities.

For lowers velocities values (3 m/s; 8.05 m/s; 10.02 m/s; and 12.55 m/s), we based ourselves on numerical and experimental work such as that of [60].

(ii) To analyse the Influence of particle size on the efficiency of a cyclone separator, we fixed three values of inlet velocity: $v_1 = 8.02$ m/s; $v_2 = 10$ m/s and $v_3 = 15$ m/s, and for each velocity value, we chose ten different particle diameters, from finest to the least fine (0.01, 0.1, 1, 2, 3, 4, 7, 10, 15, and 20 μm). Then, we calculated the different efficiencies as a function of the particle diameters, for those any three velocities as Table 8. The efficiency formula is given in (15) "number of particle tracked" represents the number of particle injected by the inlet and "number of particle trapped", the number of particle that hit the collection bin as mentioned above. If, when numerically performing steady DPM trajectory in Fluent, the calculation converges (or the maximum number of steps is reached) and a given particle still does not reach the outlet or collection bin (or escape/trap), that particle fat is reported as "incomplete". In such a case, it is probable that particle is kept churning in the re-circulation region and is not coming out the domain, thus being reported incomplete. As these particles cannot be considered as either escaped or collected, they must be subtracted from the number of particle injected when calculating the cyclone efficiency, as shown in the following formula:

$$\text{Efficiency} = \frac{\text{Number of particle trapped}}{\text{Number of particle tracked} - \text{Number of particle incomplete}} \times 100. \tag{15}$$

2.1.7. Convergence Criterion. The calculation is considered to converge when the residual stabilises [61]. Depending on the number of iterations imposed, this can happen before (fast convergence) or exactly after the number of iterations imposed.

Due to the computation time and the improvement of the results, a residual of 10^{-5} seems to be the most appropriate for a good estimation of the convergence accuracy for the different unknowns of the Navier-Stokes equations. Since for residuals of 10^{-6} and 10^{-7}, the computation is rather time consuming and leads to little improvement in the results.

The simulations were performed on an HP laptop with an INTEL(R) Core i3-4005U CPU@1.70 GHz; a 6 GHz RAM memory, and a 64 bit operating system.

2.1.8. Collection Criterion. In reality, particles are deposited on cyclone walls just after entering, and the rest are suspended in the flow and separated by the centrifugal action accomplished with particle agglomeration, while some may leave without collecting [9]. However, this reality is difficult to model in CFD, as there is no evidence on whether, when, or where a particle is collected. Particles that touched the cyclone hopper bottom were counted as collected by Kępa [62], Wan et al. [63], and Qiu et al. [64]. Ma et al. [65] assumed that particles that touched the cyclone wall were collected, while Griffiths et al. [66] considered particles that touched the conical part and the bottom walls to be collected. The assumption based on studies by Yoshida et al. [67], Gimbun et al. [27], Chuah et al. [68], and Bhaskar et al. [69] was that the particles that escaped from the cyclone bottom were collected. The number and mass of particles that escaped from the cyclone during the simulation period are also considered as collected in the literature [58, 70, 71]. In summary, the conclusions derived for the selection of particle deposition zones in cyclone separators in CFD simulations are unclear.

Another study by de Souza et al. [72] considered two particle collection criteria: particles escaped from the outlet and those that escape through the lower diameter of the cone section. The second criterion is reasonable and fits well with the experimental results of Bohnet [73], Lim et al. [74], and Yoshida et al. [75] but can overpredict fine particle collection as there is no re-entrainment from the cone bottom. However, the authors found that the grade efficiency curves do not converge after the cyclone residence time, and thus particles may bounce back and escape from the outlet, leading to an underprediction of collection efficiencies assuming particles escaping from the outlet [9]. Therefore, assuming particles that touched the hopper bottom were assumed to be collected in this study.

2.1.9. Analysis Sections. The analysis sections are the 2D sections of the model on which we will plot the profiles of the different parameters that influence the efficiency of the separator in order to analyse them. These are as follows:

(i) Section A-A: An output section in the vortex finder ($x = 0$; $y = 1.300$; $z = 0$)

(ii) Section B-B: A section of the cylinder ($x = 0$; $y = 1.125$; $z = 0$)

(iii) Section C-C: A section of the cone ($x = 0$; $y = 0.500$; $z = 0$)

(iv) Section D-D: A section of the extension of the base diameter of the cone ($x = 0$; $y = -0.100$; $z = 0$)

(v) Section E-E: A section of the collector ($x = 0$; $y = -0.300$; $z = 0$)

For the different contours, we used the planes $(0; y; 0)$; the plane ($x = 0$; $y = 1.125$; $z = 0$) and the plane ($x = 0$; $y = 1$; $z = 0$) on which we represented the smooth and/or scratched profiles to better observe the contour lines.

Those are show at Figure 5.

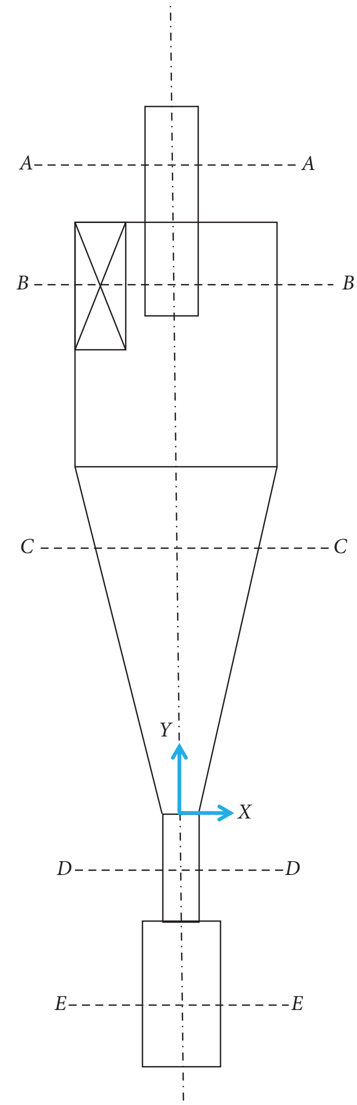

Figure 5: Study sections.

2.2. Theoretical Approach. The pressure drop in a cyclone separator plays a vital role in the performance evaluation. It is generally caused by the frictional interactions between the flowing fluid and the solid wall. The total pressure losses in a cyclone separator mainly comprise the losses at inlet, cyclone chamber and outlet. So, the proper cyclone design is very essential as it is directly related to the pressure drop. The maximum amount of total pressure drop take place over the cylindrical and conical chamber in a cyclone separator, due to energy dissipation loss by the strong swirling turbulent flow. Demir et al. [76], introduced the standard pressure drop equation for a cyclone separator, which is generally given as:

$$\Delta P = 0.5\xi_C \rho_g V_{\text{in}}^2, \tag{16}$$

where ΔP is cyclone pressure drop, ρ_g is the gas density, V_{in} is the gas velocity at inlet and ξ_C is an important pressure drop parameter, which mainly contains some dimensional correlations. There are various models are available in the literature, but in this present study, six models have been selected to predict the pressure drop including model based on estimating the dissipative loss such as Stairmand [51], and five purely empirical models such as Casal and Martinez–Benet [77], Coker [78], Dirgo [79], Shepherd and Lapple [80], and First, as shown in Table 9. The pressure drop between the inlet and outlet of a cyclone separator is the quantity of work, which is important to operate the static device for given conditions [81]. The operational cost, energy consumption and collection efficiency are directly associated with the pressured drop. The pressure drop in cyclone is directly proportional to velocity head and gas density. In these analytical models some includes the effect of cyclone body diameter, conical heights, friction factor, cross-section of inlet, gas viscosity, vortex finder diameter, and height as well. In the present work, the static pressure drop under different operating condition is predicted numerically and also validated with theoretical models and experimental model of the Stairmand 1D2D design cyclones found by Lingjuan W. [60].

To improve the efficiency, we used three models: Iozia and Leith and Dirgo and Leith model [4, 82] have an excellent record to calculate the cyclone efficiency as function of particle size at fixed velocity ($V_{in} = 10$ m/s). The mathematical expression is given in Table 10. The model basically assumes that a particle carried out by the vortex encounter two forces mainly the centrifugal force and the flow resistance. The logistic model named Iozia and Leith [82, 83] shows a good investigation with experimental data for the large cyclone size Dc = 0.25–0.4 m [83, 84]. We also used the Licht [4] model based to exponential and logarithm functions Table 10. Those three empirical models were combined with the Barth model of cut-size [4], Table 10, and the design of separator. So, these models can be used for the efficiency calculation in the cyclone separator and can be validated with numerical result for the present geometry and experimental data found by Yangyang et al. [85] with 1D2D Stairmand design cyclone.

Table 9: Empirical models of pressure drops.

Models	Numerical values	Pressure drops
Stairmand: $\xi_C = 1 + 2q^2[(2(D+b)/D_e) - 1] + 2(4ab/\pi D_e^2)^2$ $q = (\mathrm{ab}/2\mathrm{AG})[-(D_e/2(D-b))^{0.5} + ((D_e/2(D-b)) + (4\mathrm{AG}/\mathrm{ab}))^{0.5}]$ $A = (\pi(D^2 - D_e^2)/4) + \pi Dh + \pi D_e S + (\pi(D-B)/4)[(H-h)^2 + (D-B/2)^2]^{0.5}$ $G = 0.005$	$A = 1.037\,m^2$ $q = 0.9$ $\xi_C = 5.064$	$\Delta P = 3.10V_{in}^2$
Shepherd and Lapple: $\xi_C = 16(\mathrm{ab}/D_e^2)$	$\xi_C = 6.4$	$\Delta P = 3.92V_{in}^2$
Casal and Martinez–Benet: $\xi_C = 11.3((ab/D_e^2))^2 + 3.33$	$\xi_C = 5.138$	$\Delta P = 3.147V_{in}^2$
Coker: $\xi_C = 9.47\mathrm{ab}/D_e^2$	$\xi_C = 3.78$	$\Delta P = 2.32V_{in}^2$
Dirgo: $\xi_C = 20((ab/D_e^2))[(S/D)/((H/D)(h/D)(B/D))]^{(1/3)}$	$\xi_C = 4.087$	$\Delta P = 2.5V_{in}^2$
First: $\xi_C = (ab/DD_e)((12/Y))[(h(H-h)/D^2)]^{-1/3}$ $Y = 0.5$	$\xi_C = 3.09$	$\Delta P = 1.89V_{in}^2$

Table 10: Empirical models of Efficiency.

Models	Numerical values	Grade efficiency functions
Cut-size of Barth–Muschelknautz: $x_{50} = [9V_{rcs}\mu D_x/\rho_p V_{\theta cs}^2]^{(1/2)}$ $V_{\theta cs} = (V_{\theta w}(R/R_e)/(1 + (H_{cs}R\pi f V_{\theta w}/Q)))$ $V_{\theta w} = (V_{in}R_{\mathrm{in}}/\alpha R)$ $\alpha = 1 - 0.4(b/R)^{0.5}$ $H_{cs} = (H-S) - ((H-h)((D_e/2) - (B/2))/R - (B/2))$ $R = D/2$ $V_{rcs} = Q/\pi H_{cs}D_e$ $f = 0.005[1 + 3(C_o/\rho_g)^{0.5}]$ Where $C_o = 0.5$, $V_{in} = 10$, and $\rho_g = 1.225$	$x_{50} = 2.05\,\mu m$	
Dirgo and Leith: $\eta(x) = 1/1 + (x_{50}/x)^{6.4}$		$\eta(x) = 1/1 + (2.05/x)^{6.4}$
Iozia and Leith: $\eta(x) = 1/1 + (x_{50}/x)^{\beta}$ $\beta = 0.62 - 0.87\ln(x_{50}/100) + 5.21\ln(ab/D^2) + 1.05[\ln(ab/D^2)]^2$	$\beta = 9.6$	$\eta(x) = 1/1 + (2.05/x)^{9.6}$
Licht: $\eta(x) = 1 - \exp[\ln(0.5)(x/x_{50})^2]$		$\eta(x) = 1 - \exp[\ln(0.5)(x/2.05)^2]$

3. Results and Analysis

The collection efficiency and pressure drop of a cyclone separator are a direct result of the flow pattern of the gas and solid phase, as well as the pressure field within the cyclone. Based on the meantime, the dominant flow character in the cyclone is a vortical and can be described as the "Rankine vortex". It is a combination of a quasi-free outer vortex and a quasi-forced inner vortex. Apart from the gas inlet velocity and geometrical parameters, wall friction and solid particle loading also influence the strength of the vortex. Empirical models often neglect the latter two and are therefore limited in their applications. Numerical modeling is therefore necessary to understand velocity and pressure fields [12].

3.1. Pressure Field Analysis

3.1.1. Static Pressure. The static pressure variation has a relatively identical profile in all the sections of the separator (Figure 6). The maximum value of the static pressure is found in the body of the cyclone (dress), more precisely in the region of the quasi-free vortex; its intensity drops drastically from the walls to the center (region of the quasi-forced vortex) (Figure 7), due to a strong vortex velocity; then many particles can be re-entrained and escape if they enter this zone. Although the static pressure drops drastically in the radial centripetal direction, its axial variation remains small (Figure 7).

The pressure field has a stronger gradient in the radial direction because a greatly intensified forced vortex exists, while in the axial direction it remains weak. This results in the existence of two helical motions, one heading towards the base of the cyclone and the other towards the vortex finder. These two vortices are clearly visible in the axial and tangential velocity fields (Figures 8 and 9). Thus, a long region of negative static pressure exists at the center of the cyclone (Figure 6).

3.1.2. Dynamic Pressure. The dynamic pressure is highest at the cyclone inlet at the interface between the quasi-free vortex and the quasi-forced vortex (Figure 10). The dynamic pressure curve is asymmetric (Figure 11), due to the nonsymmetry of the tangential velocity profile (because the cyclone has only one inlet, and therefore the axis of the vortex cannot coincide with its geometric axis).

The dynamic pressure is high in the quasi-free vortex region and cancels out in the quasi-forced vortex region on the central axis of the cyclone (Figure 10). The same behavior is visible in the extension of the base diameter of the cone and even in the collector.

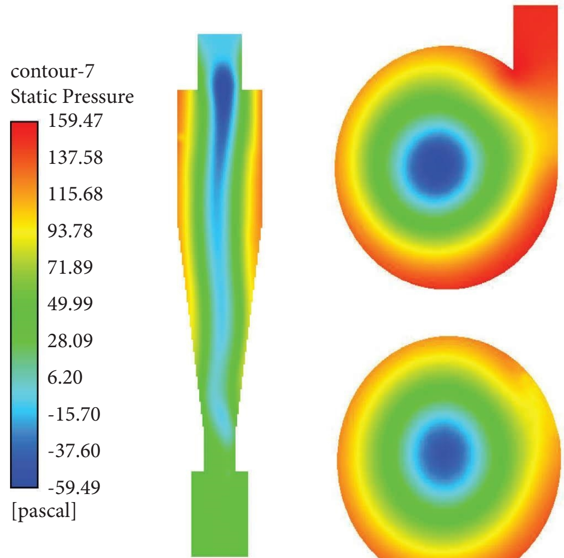

FIGURE 6: Static pressure contours.

With the extension of the base diameter of the cyclone cone, the pressure drops decrease along the vertical axis; meanwhile, with the effects of velocity nonsymmetry and especially the tangential velocity, which dominates the vortex flow field, the dynamic pressure remains nonaxisymmetric [9].

The dynamic pressure profile is closely related to that of the tangential component of the mean velocity: the higher the mean velocity, the higher the dynamic pressure.

3.2. Flow Field Analysis

3.2.1. Average Speed Intensity. The contour of average speed intensity is presented on Figure 12. Of the three velocity components in the vortex flow inside the cyclone, the tangential component is the largest which governs the flow pattern and separates particles by centrifugal force [86].

The axial flow is also important for the transport of particles collected from the walls to the base collector. In cyclone aerodynamics, the radial velocity is the weakest component [9], although it contributes to the transport of the collected particles from the walls to the collector with the effect of the centripetal force and also contributes largely to the return of the quasi-forced central vortex [2].

3.2.2. Axial Velocity. The axial velocity is of major influence in the transport of solid particles towards the collection device. The empirical model based on the double vortex structure postulates constant values for the downward flow in the outer vortex (quasi-free) and the upward flow in the inner vortex (quasi-forced) [12, 64]. These values cancel at the axial position where the vortices end.

In fact, the numerical analysis shows us that the axial velocity contour has a positive downward flow and a negative upward flow (Figure 8). These flows are helical in the cone and its extension and even in the collector, allowing a rapid transport of solid particles towards the collector. But these helical flows can also allow a re-drainage of the particles towards the vortex finder, thus contributing to a decrease in the efficiency of the cyclone. Also, the contour is not flat (uniform) (Figure 13), but has maxima and minima. Typically, the outer flow shows maxima in the vicinity of the edges, while the inner flow chows a minimum in the vicinity of the cyclone geometry axis.

The diameter of the quasi-forced inner vortex of the gas entering the vortex finder is larger than that of the vortex finder; as a result, the gas velocity drops drastically in the vortex finder at the center, at the exit of the separator. This can contribute to increase pressure drops [2].

The axial velocity component is not axisymmetric and is directed upward out of the cyclone walls and downward inside the cyclone core (Figure 13). The upward and downward maxima are always less than the inlet velocity for any study [7].

3.2.3. Tangential Velocity. The typical tangential velocity contour is shown in Figure 9.

The distribution of tangential velocity is similar to that of the dynamic pressure (Figure 10). This shows that the tangential velocity is the most dominant velocity component in the cyclone separator [87]. For the same reasons, the magnitude contour of the average velocity is almost similar to that of the tangential velocity (Figure 12). Consequently, the tangential velocity dominates the flow, and the intense shear in the radial direction. This results in a centrifugal force, which determines the separation of the particles.

It was observed that the inlet velocity is accelerated due to the geometry of the cyclone and its value increases from its initial value, and then decreases as the gas swirls towards the base along the cyclone separator and reaches its minimum in the center of the cyclone (Figure 9). At the certain cross-section within the cone (diameter less than or equal to that of the vortex finder), there is a reversal of flow and the

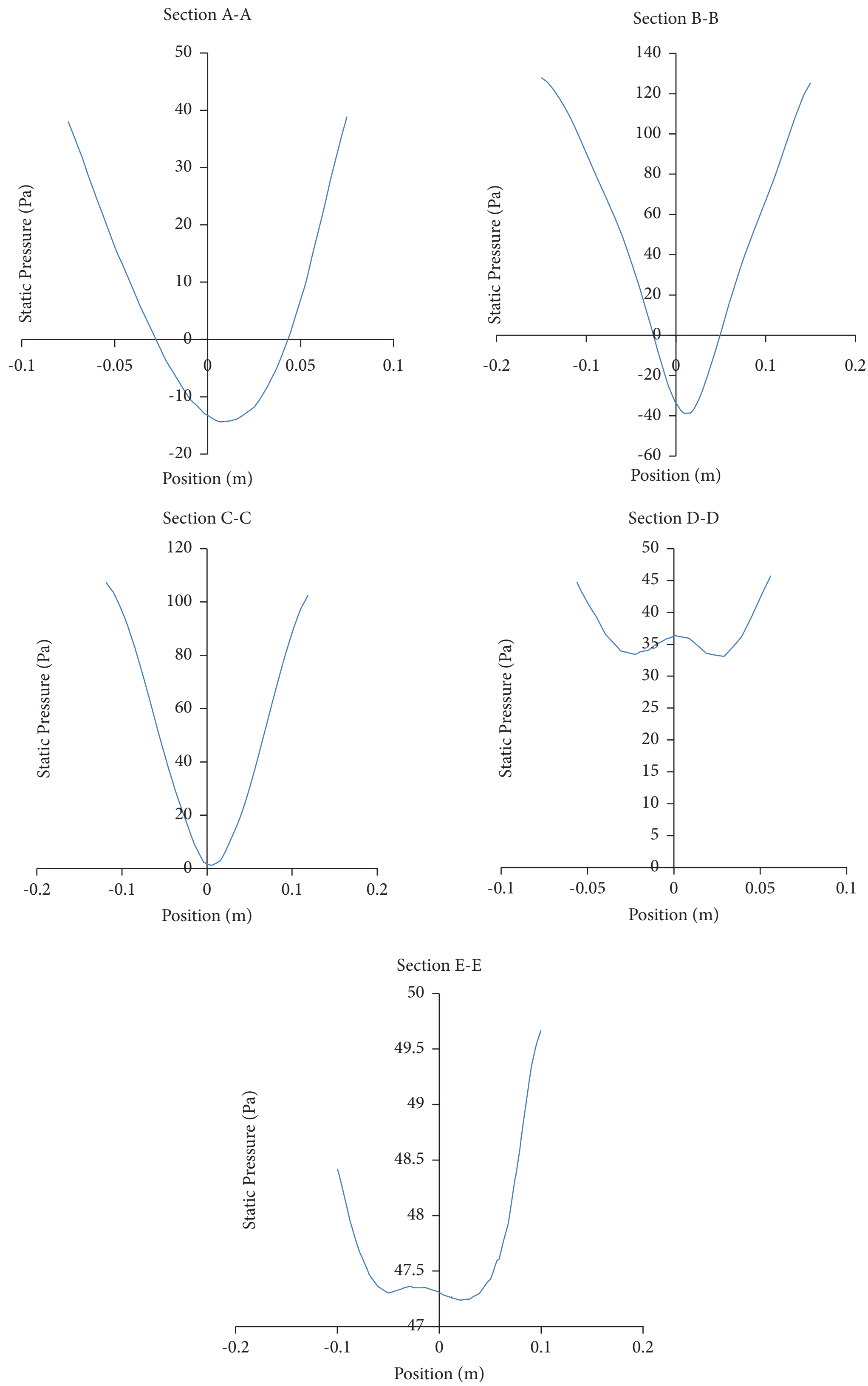

Figure 7: Static pressure curve as a function of the analysis section.

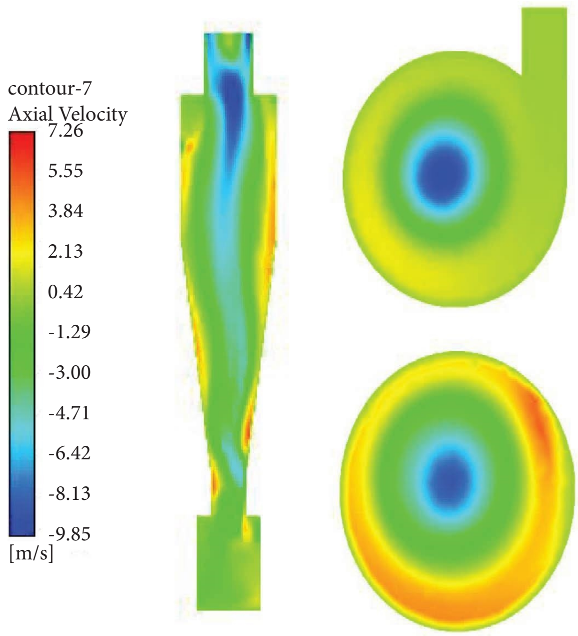

Figure 8: Axial velocity contours.

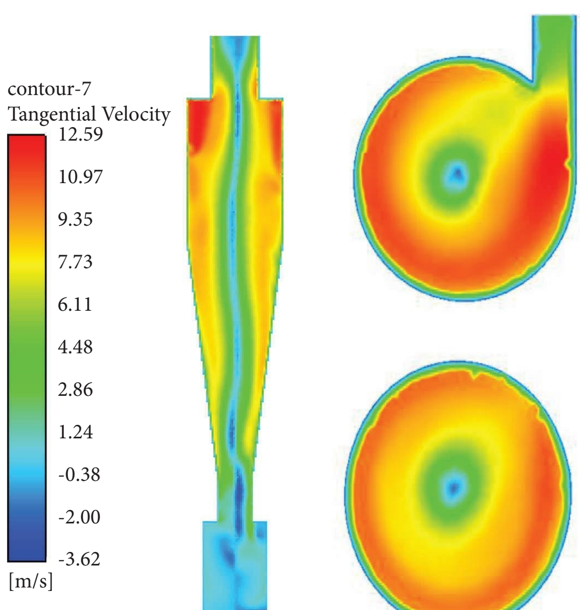

Figure 9: Tangential velocity contours.

gas flows opposite direction. Before entering the vortex finder, the gas in the quasi-forced return vortex collides with the continuous flow; this result in a chaotic flow just below the vortex finder, and the speed drops sharply (Figure 9). This causes energy losses and pressure drops.

The tangential velocity is highly dependent on the geometry of the cyclone, the frictions and the particle loading [12].

The tangential velocity contour (Figure 9) shows the so-called "Rankine vortex" which consists of two parts: an intense or quasi-free outer vortex and an inner or quasi-forced

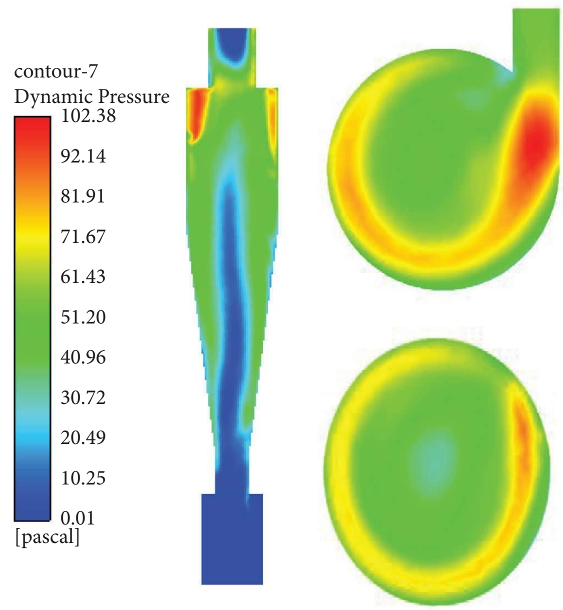

Figure 10: Dynamic pressure contours.

vortex. The tangential velocity profile [88] (Figure 14) is relatively similar at different sections within the same cyclone separator; these profiles show that the velocity is zero at the cyclone walls, reflecting the removal of solid particles from the downward vortex flow (Figure 14). It can be also be seen that in the outer region of the quasi-free vortex, due to a rapid decrease in the tangential velocity intensity (almost zero) in the vicinity of the walls, the distribution is different at each section and the change in the value of the maximum tangential velocity is relatively limited [7, 88].

Generally, the tangential velocity distribution varies only slightly with the axial position in the cyclone (Figure 14) [57]. This means that if the tangential velocity increases in one section of the cyclone, it will also increase in all other sections.

3.2.4. Radial Velocity. The radial velocity affects the deflection of particle. This is an important factor in the analysis of particle collection and cyclone efficiency. Analytically, the radial velocity is considered to be the average velocity component with the lowest value [64]. However, this is only valid for the inner or quasi-forced vortex, and especially in the vicinity of the vortex finder, where it grows rapidly towards the core of the vortex [12, 89].

The radial velocity contour is given in Figure 15. This contour is helical. The axis of the vortex is slightly curved and not aligned with the geometric axis of the cyclone. It can be seen from Figure 16 that the radial velocity contour is positive on one side and negative on the other, alternating along the separator. This is due to the fact that the cyclone separator with a single tangential inlet is nonaxisymmetric. It is also observed that the radial velocity increases sharply towards the core of the vortex at the inlet of the separator. Alekseenko [12] suggested that this phenomenon is the result of the helical rotation of the vortex along the flow around the geometric axis of the cyclone (Figure 15).

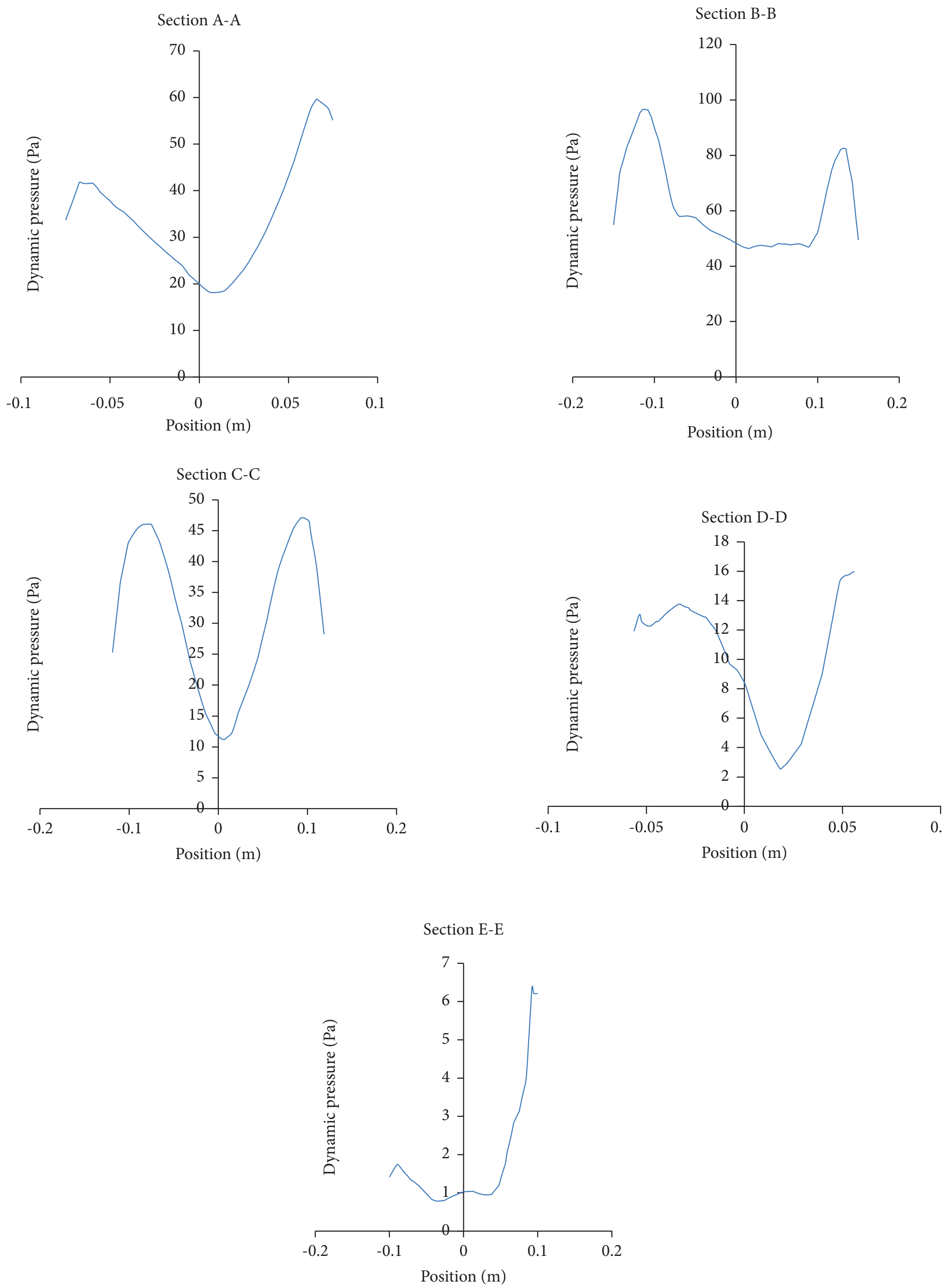

Figure 11: Curves of dynamic pressure according to the section of analysis.

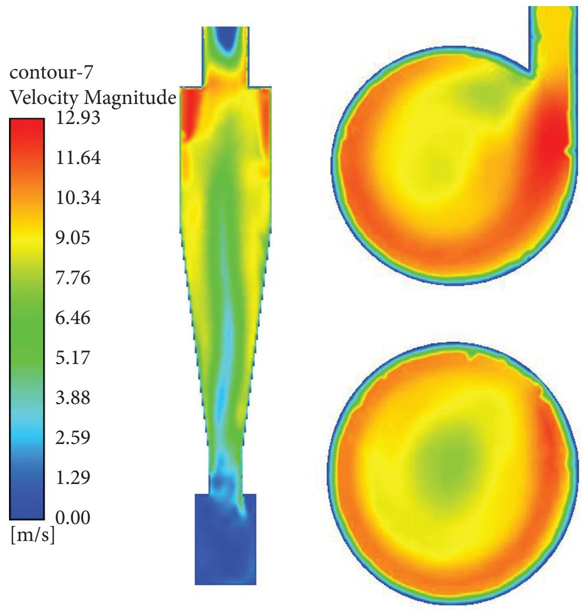

FIGURE 12: Velocity intensity contours.

It is also observed that as the distance from the base of the separator increases, so does the radial velocity intensity in the quasi-forced vortex, which accelerates the helical rotation of the inner vortex (Figures 15 and 16). These two factors contribute to a re-entrainment of some (finest) particles and therefore to the decrease of the cyclone separator efficiency.

The radial velocity contour shows that it is negative in the gas at the inlet to the separator and quickly becomes zero. Then, it becomes positive due to the centrifugal force and the acceleration of the mean velocity (due to the geometry of the separator) around the vortex finder.

Finally, the radial velocity profile in the vortex finder (parabolic pointing upwards) (Figure 16 section A-A) shows that it is largely the mean velocity component responsible for the backflow.

3.3. Influence of the Flow Rate (Inlet Velocity) on the Pressure Drops and Efficiency of a Cyclone Separator. The curve of pressure drops and efficiency as a function of the inlet velocity are presented in Figure 17. They present parabolic profiles. The pressure drop and collection efficiency in the cyclone separator are related to each other (Table 11).

The pressure drops and efficiency across the cyclone separator increases closely with the inlet velocity of the separator. It is therefore higher for higher inlet velocity and lower for lower ones.

The particle collection efficiency is the most significant index by which the cyclone performance can be evaluated. The collection efficiency of a cyclone separator is known as the particle capture rate, which is the ability to separate the solid inert particles from the gas stream. There are many important factors, that affects the overall collection efficiency such as density of solid particle, particle diameter, gas velocity (in this study), gas temperature, cyclone dimensions, and pressure drop.

In the cyclone separator, high-speed flow enters from the inlet, and particles are subjected to an inwardly directed drag as well as an outwardly directed centrifugal force in barrel section. Particles directly attack on the cylindrical wall and create a swirling motion around the gas outlet inside the cyclone chamber (tangential velocity). So, the gas starts following an outer vortex shaped pathway and particles falls down in the collection bin, in a helical manner (axial velocity). Finally, the light gas moves upward or discharged through the outlet tube with fine particles, following an inner vortex (radial velocity). The centrifugal force is directly proportional to the mass of the particle. It is assumed that the particle velocity is same as that of gas flow. When the particles are suspended in a fluid flow, the phenomenon can be characterised by a dimensionless number named Stokes number, which is the ratio of the characteristic time of a particle to the fluid flow. The mathematical expression is written as

$$\mathrm{Stk} = \frac{t_0 V_{\theta w}}{D}, \tag{17}$$

where t_0 is the relaxation time of the particle, $V_{\theta w}$ is the flow velocity and D is the cyclone diameter [90]. The characteristic time of the particle is given as

$$t_0 = \frac{\rho_p d_p^2}{18\mu_g}, \tag{18}$$

where ρ_p is the particle density, d_p is the diameter of particle and μ_g is the fluid viscosity. For the accurate tracing, the response time of particle should be faster compared to the smallest time scale of the fluid flow. So, smaller the value of stokes number, produce acceptable tracing accuracy. When

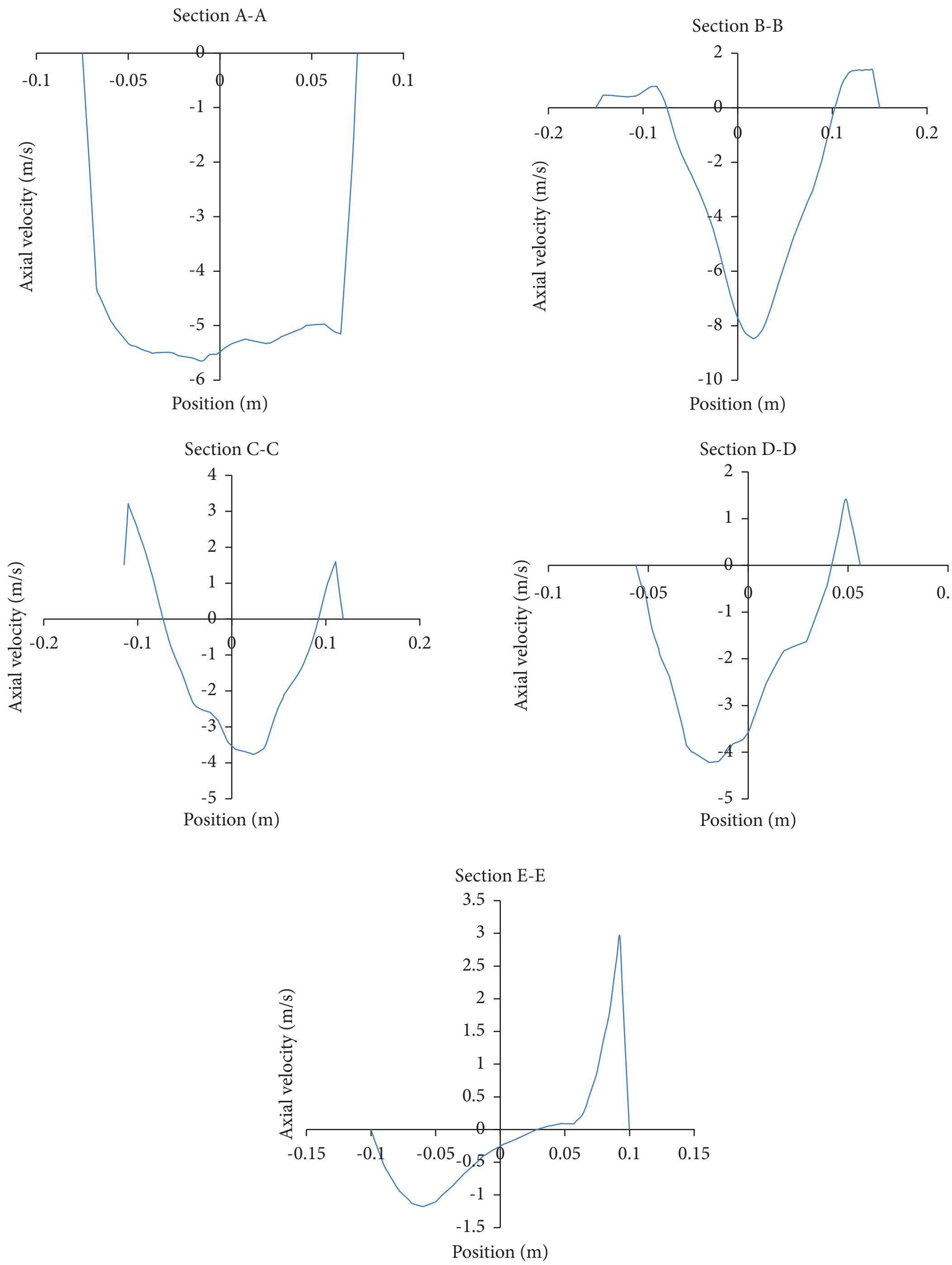

Figure 13: Axial velocity curves depending on the analysis section.

Stk ≫ 1, the particles are detached from the fluid flow and for Stk ≪ 1, particles follow the fluid flow properly. But for Stk < 0.1, the tracing accuracy is high with less than 1% error [83]. So, we can conclude that, when the inlet velocity increases, the flow velocity increases, and so does the Stokes number, which helps to improve efficiency.

The pressure drop in a cyclone can be described as the amount of energy required to operate the system by moving the flowing gas through the inlet and outlet of the static device. So, the separation efficiency is associated with the pressure drop, which helps to estimate the operating cost of a cyclone separator.

The main part of the pressure drop, i.e., about 80%, is considered to be pressure losses inside the cyclone due to the energy dissipation by the viscous stress of the turbulent rotational flow [81, 83]. The remaining 20% of the pressure drop are caused by the contraction of the fluid flow at the outlet, expansion at the inlet and by fluid friction on the

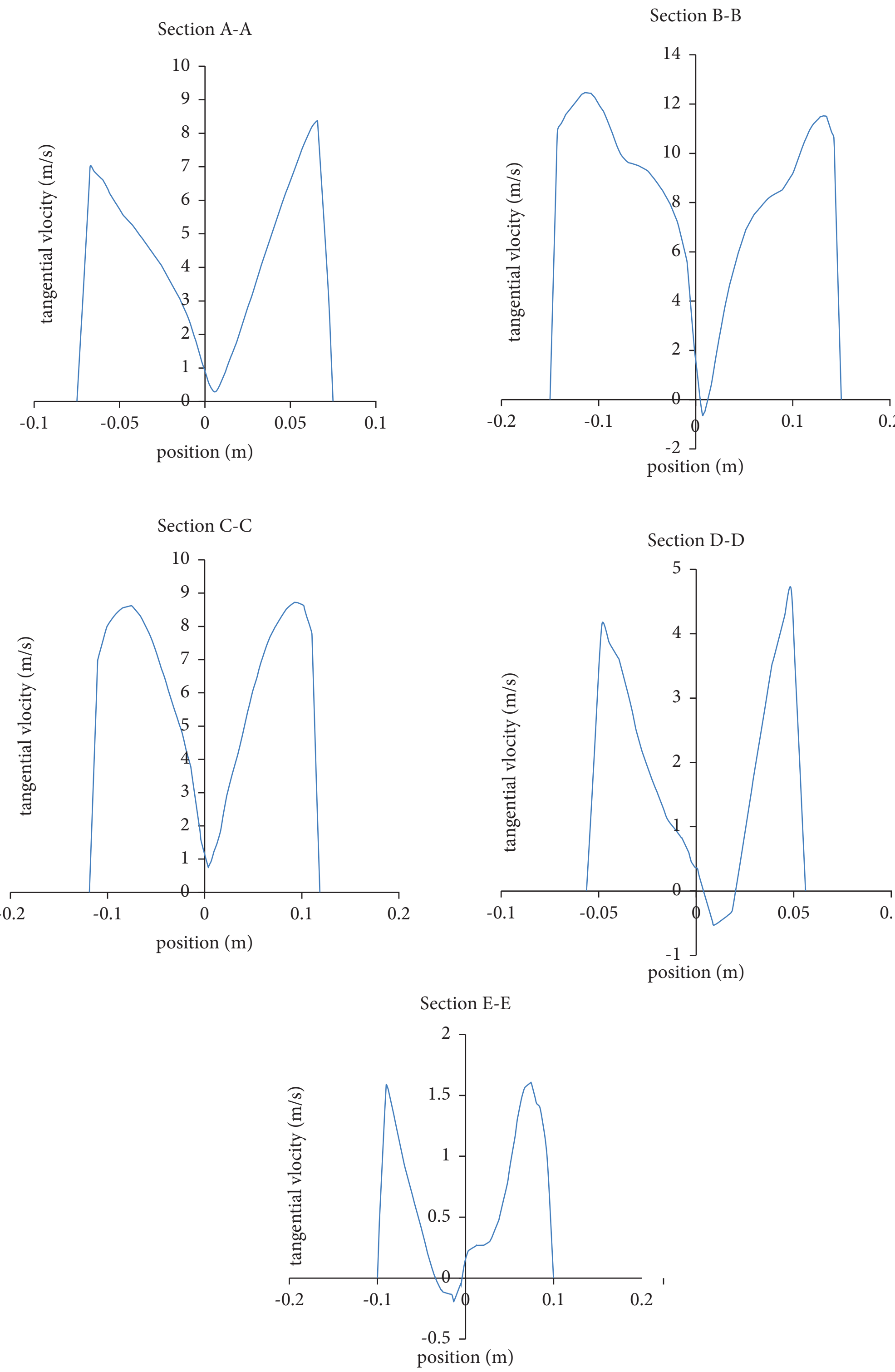

Figure 14: Curves of tangential speed according to the section of analysis.

cyclone wall surface. Pressure drop or flow resistance is strongly dependent on flow velocity. As the velocity increases, Reynold's number also increases, resulting in intense turbulence and shocks between particles in flow. The result is an increase in efficiency, but also an increase in pressure drop, as shown in Table 11 and Figure 17.

In conclusion, efficiency and pressure drops increase with inlet velocity into the cyclone dust separator, one being positive impact and other negative. A balance therefore needs to be struck at the design stage in terms of available energy and the desired efficiency range, in order to choose the best inlet velocity for an application.

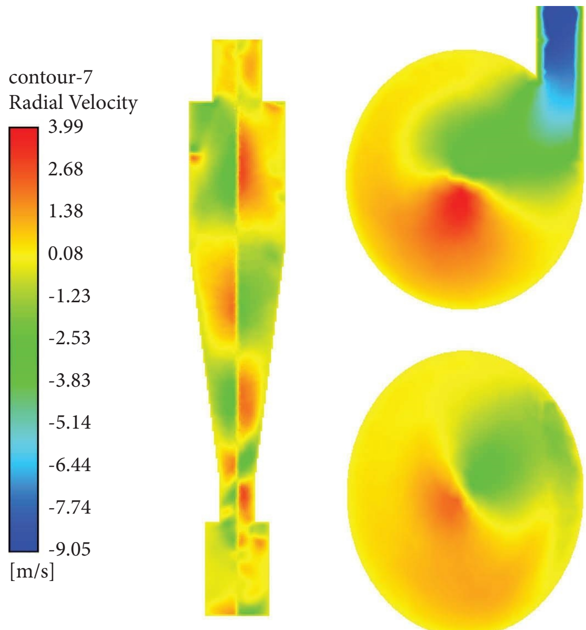

FIGURE 15: Radial velocity contours.

In order to better understand the behavior of the pressure drops as a function of the gas inlet velocity in the separator, we will plot the curve of the natural logarithm of the pressure drops $\ln(\Delta_P)$. Table 12 presents the values of $\ln(\Delta_P)$ as a function of $\ln(v)$.

The profile of the curve of the Neperian logarithm of the pressure drops $\ln(\Delta_P)$ is a straight line (Figure 18), proof that the pressure drops in the cyclone are exponent functions of the speed.

We can then obtain by calculating the slope of the line: $\ln(\Delta_P) = 2.0007 \ln(v)$.

It can then be concluded that the variation of the pressure drops as a function of the inlet velocity can correspond to the first order theoretical formulation which is in the form:

$$\Delta_P = Av^2, \tag{19}$$

where A is constants and v the speed; we can therefore validate the agreement with the theoretical expression:

$$\Delta_P = 0.5\xi_C \rho_g V_{\text{in}}^2, \tag{20}$$

where ξ_C is an Euler number, ρ_g is density and is inlet velocity.

3.4. Influence of Particle Size on the Efficiency of a Cyclone Separator. The curves obtained are shown in Figure 19.

The summary of the different efficiencies as a function of the diameters for any three speeds $v_1 = 8.02$ m/s (Efficiency $E1$); $v_2 = 10$ m/s (Efficiency $E2$) and $v_3 = 15$ m/s (Efficiency $E3$) is presented in Table 13.

3.5. Interpretation

3.5.1. Interpretation 1. The efficiency curve of a cyclone dust collector separator (for a given inlet velocity) as a function of particle size is strictly increasing and shows three main zones (Figure 19):

(i) A light growth zone for particles between 0 and 2 μm, corresponding to ultrafine particles. For these particles, the efficiency is very low (less than 25%), and the cut-off diameter is large. For particle sizes in this zone, it would be wise to combine the cyclone separator with other filtering devices, in particular bag filters, even if there are expensive to maintain, but it is also possible to combine several cyclones in series to increase the separation efficiency, in order to reach the required rejection threshold.

(ii) A steep growth zone corresponding to fine particles of a size between 2 and 10 μm: the efficiency of a separator in this zone can be between 25% and close to 95% for a fixed speed, depending on the average size of the particles. The cut diameter is also average there.

(iii) This is a zone that offers a significant advantage in the analysis of the efficiency of a cyclone separator and hence its design, as it can allow the desired efficiency to be obtained just by changing (incrementing or decrementing) the inlet velocity, which may include costs on the flow generator (fan or any other mechanical device). Most of the particles discharged by industries have sizes within this range, making the cyclone separator one of the most requested elements in industry for this purpose.

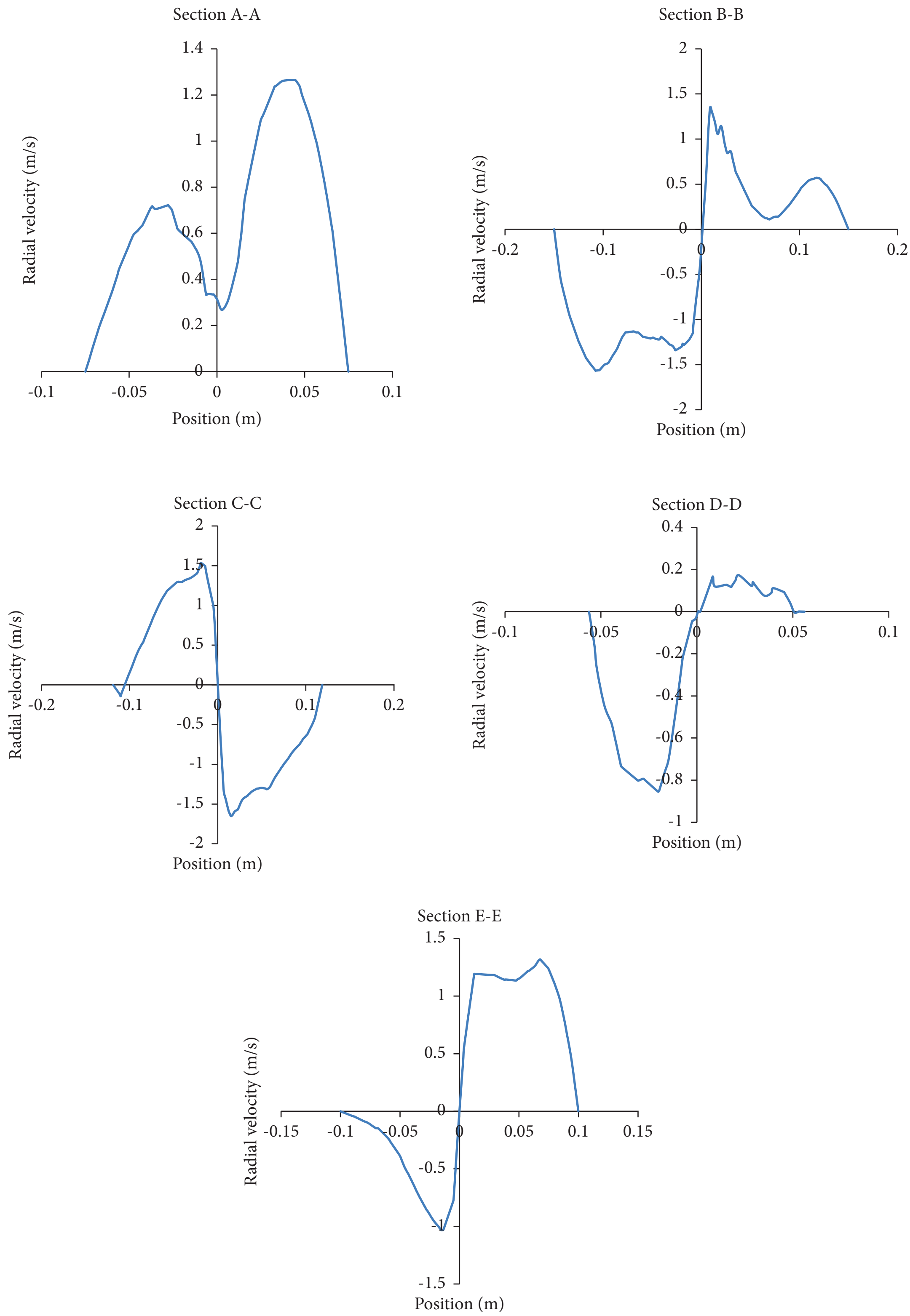

Figure 16: Curves of radial velocity as a function of the analysis section.

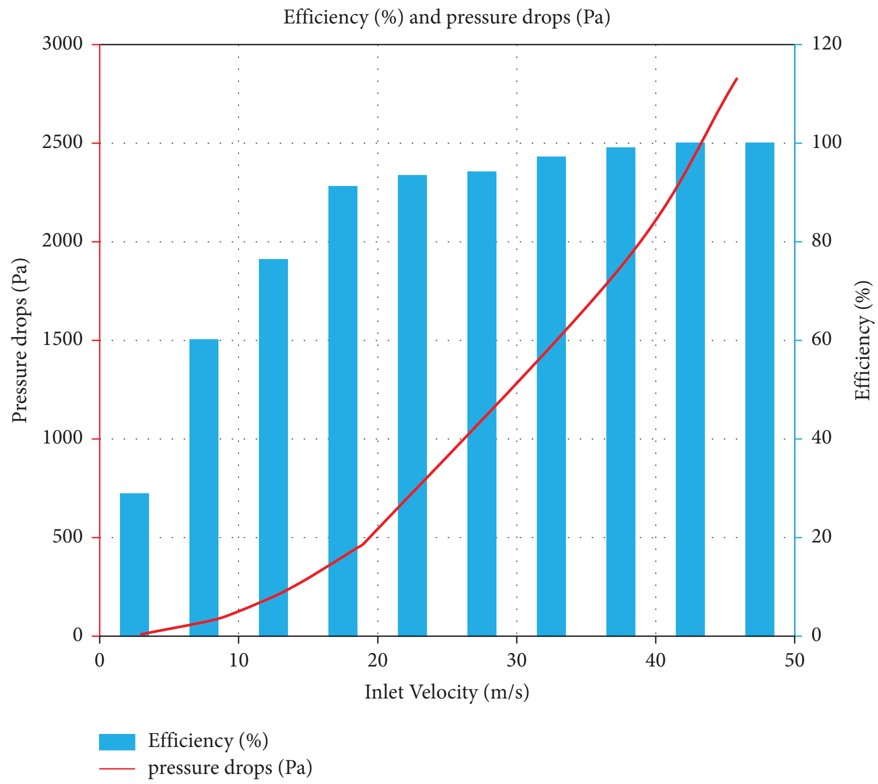

FIGURE 17: Plot of pressure drops and efficiency versus inlet velocity.

TABLE 11: Efficiencies and pressure drops as a function of speeds.

Velocity (m/s)	3	8.05	10.02	12.55	13.72	15.27	18.55	19.05	37.72	45.83
Pressure drops (Pa)	10.02	79.92	126.68	201.94	243.24	305.47	449.01	472.89	1892.76	2826.65
Efficiency (%)	28.83	60.08	76.33	91.2	93.4	94.12	97.18	99.01	100	100

TABLE 12: Values of $\ln(\Delta_p)$ as a function of $\ln(v)$.

Ln (v)	1.01	2.08	2.3	2.53	2.6	2.72	2.92	2.94	3.63	3.83
Ln (ΔP)	2,305	4,381	4,841	5,308	5,494	5,722	6,107	6,158	7,546	7,947

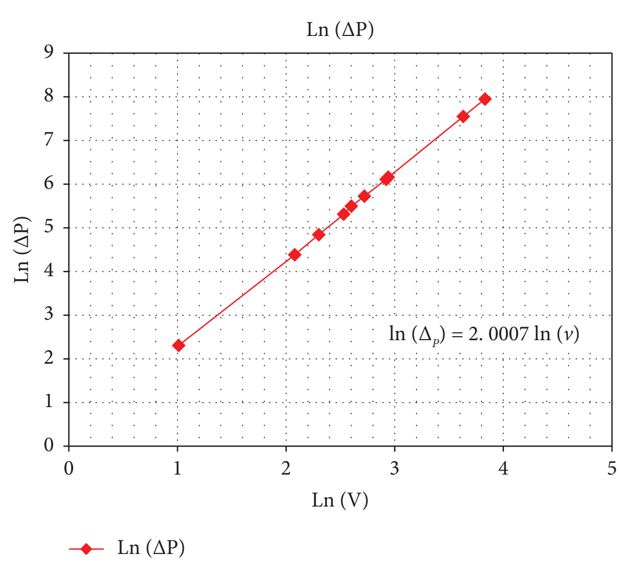

FIGURE 18: Curve of the natural logarithm of the pressure drop $\ln(\Delta_p)$ as a function of $\ln(v)$.

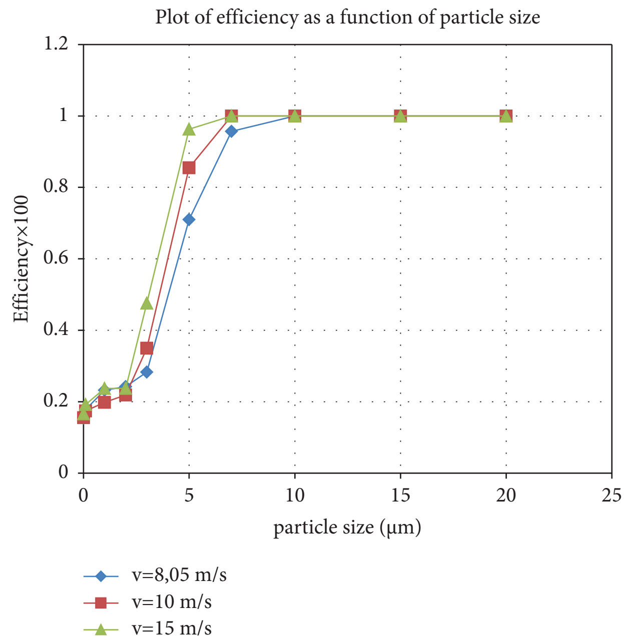

FIGURE 19: Efficiency curve as a function of particle size.

TABLE 13: Grade efficiency as function of particle size.

Diamèter	0.01	0.1	1	2	3	5	7	10	15	20
Efficiency E1	0.154	0.178	0.232	0.242	0.283	0.71	0.957	1	1	1
Efficiency E2	0.155	0.174	0.198	0.219	0.35	0.855	1	1	1	1
Efficiency E2	0.166	0.192	0.237	0.237	0.476	0.963	1	1	1	1

(iv) A constant zone or convergence zone; this corresponds to particles of size greater than or equal to $10\,\mu$m. All particles in this zone have efficiency greater than 95%. Therefore, almost all particles larger than $10\,\mu$m are collected by the cyclone separator if they are in the exhaust gas stream.

3.5.2. Interpretation 2. It is also observed in Figure 19 that the efficiency of a cyclone separator dust collector varies in increasingly with the particle inlet velocity for any fixed diameter. Thus, the higher the inlet velocity, the more particles contained in a waste air stream are likely to be captured in the separator.

These phenomena can be explained physically by centrifugal force:

$$\begin{aligned} F_c &= \frac{m{V_c}^2}{r} \\ &= m\omega^2 r \text{ with} \\ V_c &= r\omega^2. \end{aligned} \tag{21}$$

Thus, for a given particle of diameter $D = 2r$, increasing V_c amounts to increasing $\omega^2 = V_c/r$ and therefore also increasing F_c, hence the increase in efficiency as a function of inlet velocity.

On the other hand, increasing the size of the particles means to increasing their mass, which also leads to an increase in efficiency for a given fixed inlet velocity.

It can be observed that the experimental profile is similar to that obtained in our study. In terms of particle size, these models predict a convergence from $10\,\mu$m and an abrupt growth of around $1\,\mu$m which also coincides with our simulation results.

3.6. Comparison of the Three Numerical Models in terms of Contours, Efficiency, and Pressure Drops

3.6.1. The Influence of Inlet Velocity. It (Figure 20–22) shows that the RSM turbulent model has a higher pressure drop than K-epsilon turbulence models (standard and RNG). It also should be noted that this model has a higher efficiency at constant inlet velocity than the last two models. As for RNG model, it efficiency and pressure drop are higher than those of the standard model at constant velocity (Figure 21). At high inlet speeds ($V_{\text{in}} > 10$ m/s), all tree models are perfectly efficient.

Those observations can be justified by the fact that, the Reynolds stress model (RSM) is the most classical turbulence model in which the individual stress tensors are computed directly. The directional effects and the complicated turbulence flow interactions are strongly taken into account in the RSM model. However, the standard k-epsilon and RNG

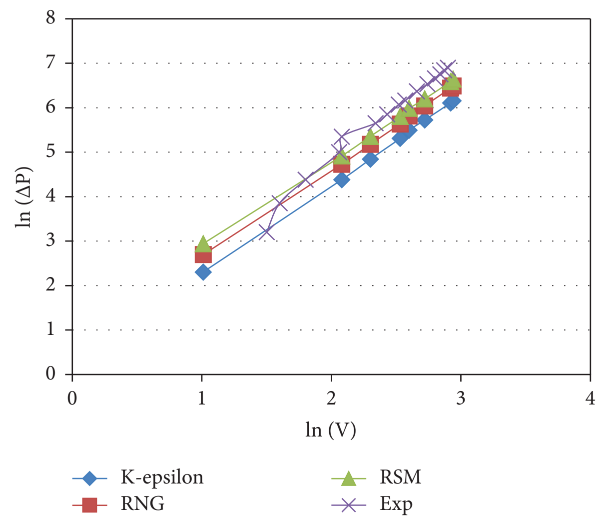

FIGURE 20: Grade logarithmic deviation between numerical pressure drops and experimental data.

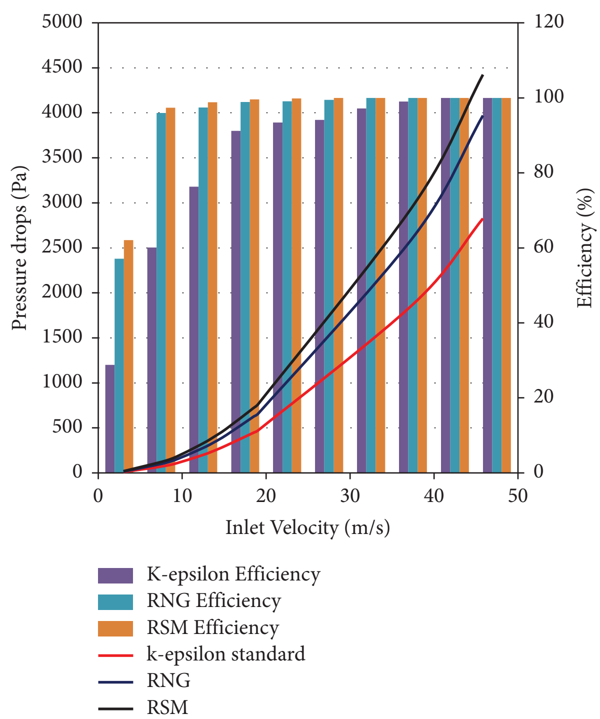

FIGURE 21: Comparison of the three numerical models in terms of pressure drop and efficiency as function of inlet velocity.

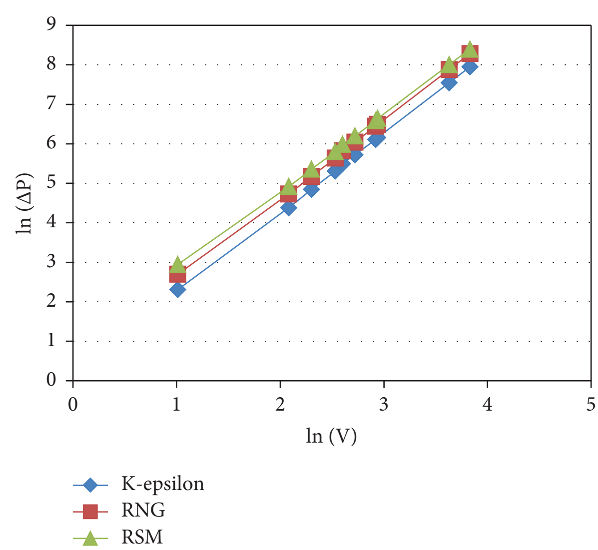

FIGURE 22: Grade logarithmic deviation between numerical pressure drops.

k-epsilon models are not suitable for swirling flows, which has anisotropic turbulence, and these models underpredicts the performance [81, 83].

Then, the RSM model constitutes a closed *N-S* equation in three-dimensional flow, which can more accurately simulate the strong cyclone flow in the internal flow field of the cyclone separator.

It is shown that good agreement of the CFD numerical calculation when compared with experimental data and predictions from empirical correlation. The results show that the CFD prediction by using the Fluent code can be used for pressure drop evaluation in cyclone design. The Fluent code with the RSM turbulence model, predict very well the pressure drop in cyclones and can be used in cyclone design for any operational conditions (Figures 21–24). In the CFD numerical calculations, a small pressure drop deviation was observed, with less than 30% of deviation at different inlet velocity which probably in the same magnitude of the experimental error of Lingjuan W. [60]. The CFD simulations with RNG *k*-epsilon turbulence model still yield a reasonably good prediction (Figures 20, 21, 23, 24) at lower velocity with the deviation about 35–38% of an experimental data. It considerably tolerable since the RNG *k*–model is much less on computational time required compared to the complicated RSM turbulence model. In all cases of the simulation, the RNG *k-epsilon* model considerably underestimates the cyclone pressure drop as revealed by Griffiths and Boysan [66].

The cyclone pressure drop can be rewritten as a function of inlet velocity head. The empirical model used for the

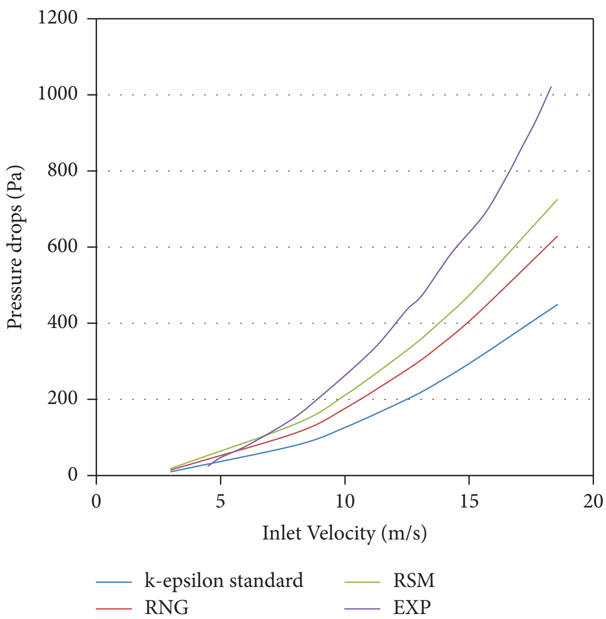

Figure 23: Comparison of the three numerical models and experimental data in terms of pressure drop as function of inlet velocity.

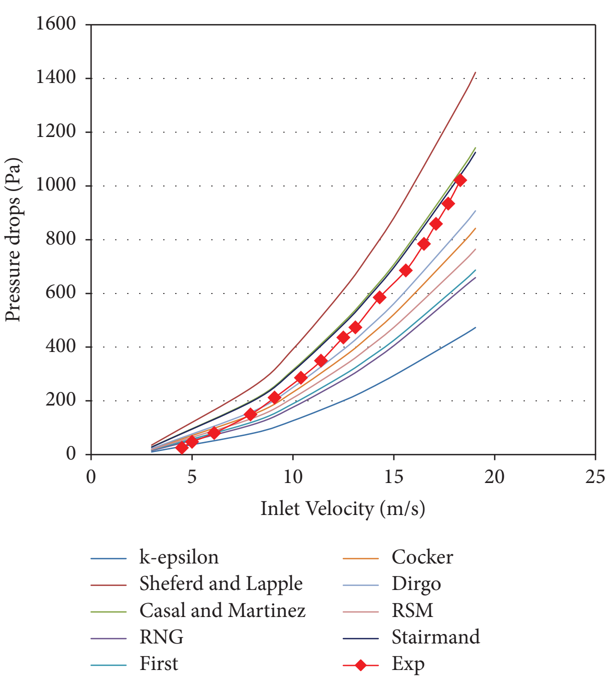

Figure 24: Comparison of the numerical, empirical, and experimental models in terms of pressure drop as function of inlet velocity.

prediction of pressure drop is much depends on the cyclone operating condition. Stairmand [51], Casal and Martine–Benet [77], and Dirgo [79] models show a good prediction on cyclone pressure drop under different operational inlet velocity (Figure 24), the prediction within 6–20% of the measured value. The deviation between RNG K-epsilon and the First model is less than 3% (Figures 24 and 25), so this

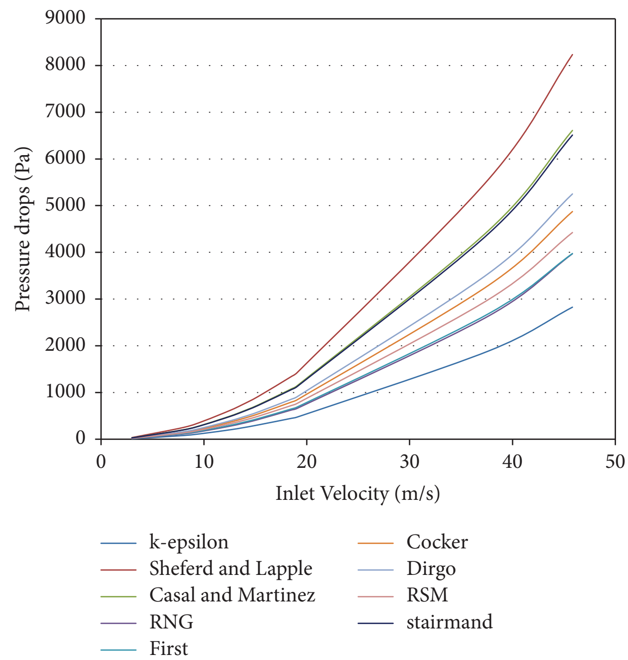

Figure 25: Comparison of the numerical and empirical models in terms of pressure drop as function of inlet velocity.

empirical model can be use at its place if one does not want to compute.

3.6.2. The Influence of Particle Size. The RSM turbulence model has higher efficiency than that given by the K-epsilon models for a given particle size (Figure 26); this is undoubtedly due to the reasons mentioned above. On the other hand, there is a gap (max value 50%) between this model and the experimental data of Yangyang et al. [85] (this could be the maximum margin error found by Yangyang T. et al. in their experiment) for fine particle ($\leq 3\mu m$) (Figure 26). The RNG model presents a curve almost similar to that of the RSM model, in the second zone of the curve (steep growth zone) (Figure 26). The curves of the empirical models are in perfect agreement with each other and show very good agreement with experimental model (Figures 27 and 28), but show a high gape with the numerical models (Figure 28). The numerical model that best approximates the empirical models at low particles size is once again, the RSM model. This can therefore be used when analysing efficiency as function of the particle size. The RNG model, whose calculation time is more reasonable than one of the RSM model can also be used in the case of law machines resources.

3.7. The Contours. Observation of the different contours of mean velocity and pressure fields (Table 14) shows us that, the Reynolds stress turbulence model (RSM) proves to be relatively successful in detecting the different aspects of rotational flow inside the cyclone separators such as anisotropy of the turbulence, presence of quasi-free and quasi-forced vortices, and the behavior of the core formed at the

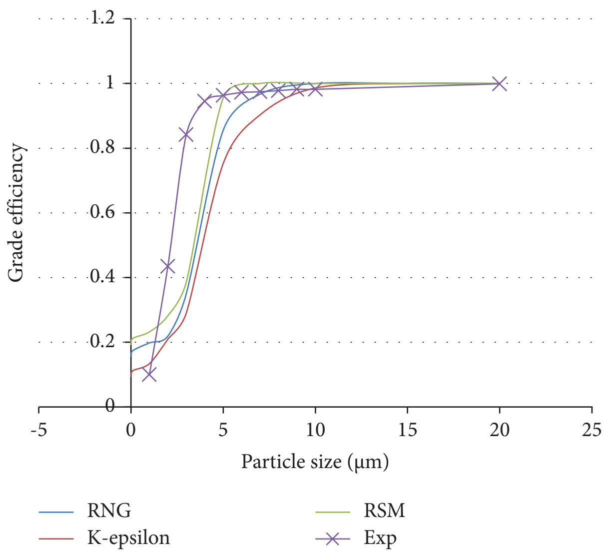

Figure 26: Comparison of the three numerical models and experimental data in terms of efficiency as function of particle size at 10 m/s.

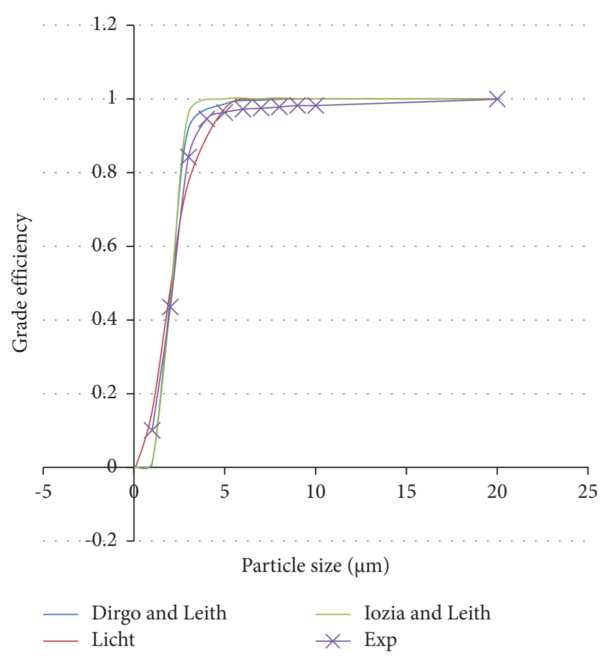

Figure 27: Comparison of the three empirical models and experimental data in terms of efficiency as function of particle size at 10 m/s.

central region, with respect to the RNG k-ε model. This model better predicts the law of the walls. On the other hand, the RNG model predicts greater maximum value of dynamic and static pressure (offset of 3.75% for static pressure and 4.68% for dynamic pressure), but the measurement of the value of static pressure between inlet and the outlet

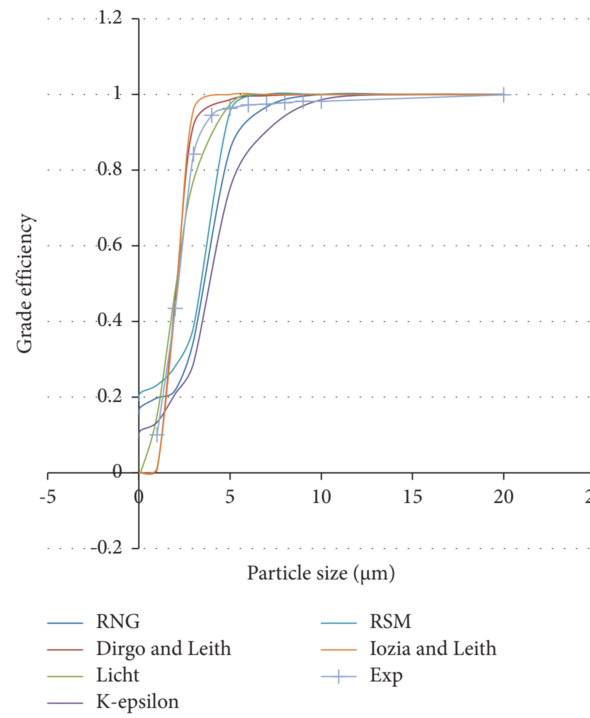

Figure 28: Comparison of empirical, numerical models, and experimental data in terms of efficiency as function of particle size at 10 m/s.

(pressure drop) remains lower than that given by the RSM model. It is the same observation for tangential velocity (offset of 3.06 %). This could be explained by the fact that the RNG model does a better job of calculating the turbulent kinetic energy and its dissipation (Tables 14 and 15), whereas the Reynolds stress model requires the solution of transport equations for each of the Reynolds stress components as well as for dissipation transport without the necessity to calculate an isotropic turbulent viscosity field (Tables 14 and 15). This is in perfect harmony with the numerical studies carried out by Fredriksson [91] which reveal that the RNG *k*-epsilon model underestimates the variation of the axial velocity profile across the radial direction and also overestimates the magnitude of the tangential velocity and the cyclone pressure field. The Reynolds stress turbulence model yields an accurate prediction of swirl flow pattern, axial velocity, tangential velocity, and pressure drop on cyclone simulations [33, 46, 91, 92].

3.8. Trajectory of a Particle inside the Separator. The trajectory of a particle inside the cyclone separator is shown in Figure 29. It can be seen that a particle takes on average 7 s to be captured in the collector; note a region of very strong vorticity at the extension of the lower diameter of the cone. This strong vorticity is intended to prevent the particle from entering the quasi-forced vortex and being re-entrained.

Table 14: Comparison of the three numerical models in terms of pressure and velocity contours at V = 10m/s.

Models	Static pressure	Dynamic pressure	Axial velocity	Tangential velocity	Radial velocity
K-epsilon standard model	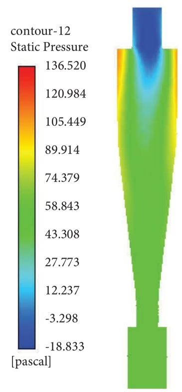	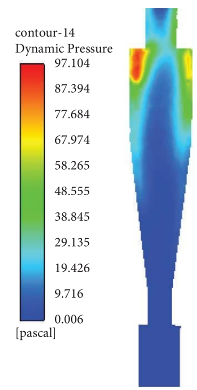	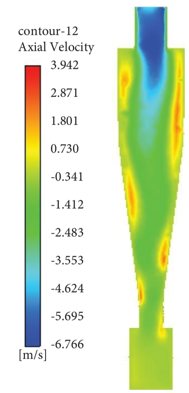	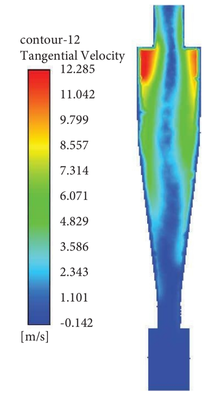	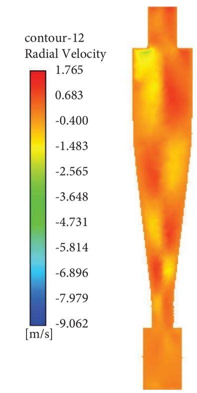
RNG-K-epsilon model	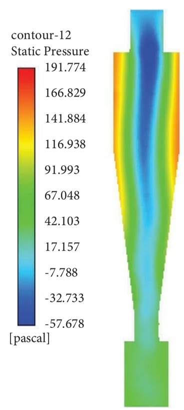	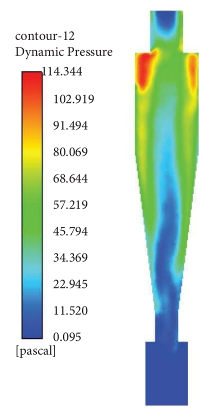	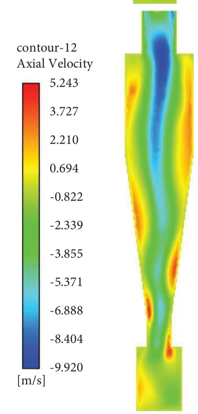	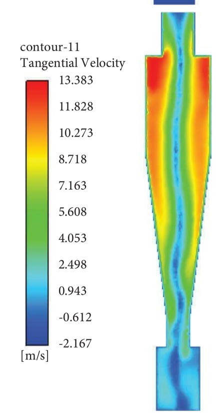	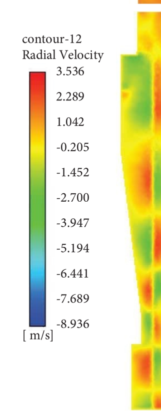
RSM-model	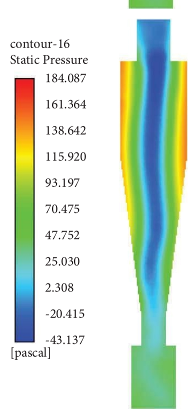	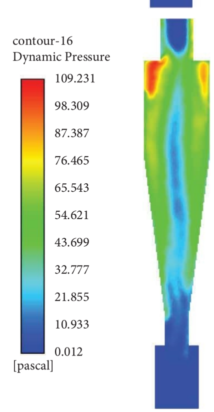	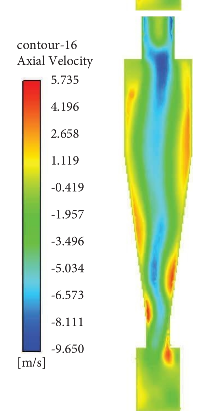	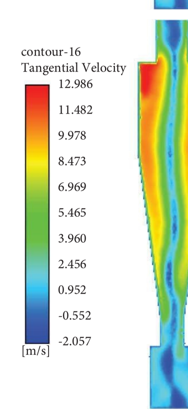	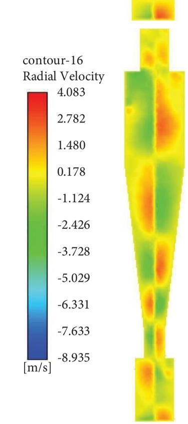

Table 15: Comparison of the three numerical models in terms of turbulent kinetic energy and turbulent dissipation rate at V = 10m/s.

<table>
<tr><th>Models</th><th>K-epsilon standard</th><th>RNG-K-epsilon</th><th>RSM-model</th></tr>
<tr><td>Turbulent kinetic energy</td><td>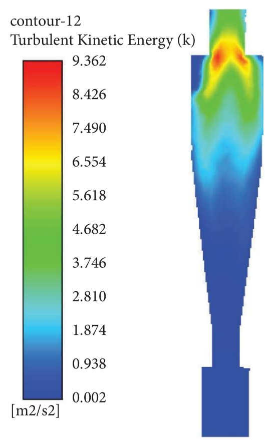
</td><td>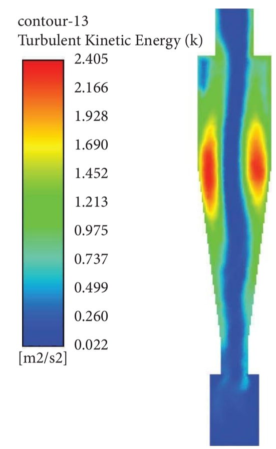
</td><td>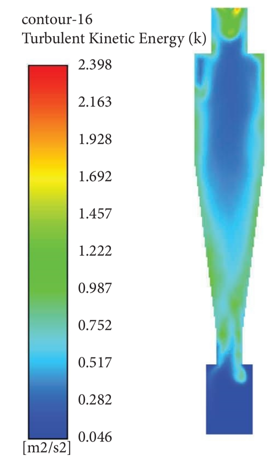
</td></tr>
<tr><td>Turbulent dissipation rate</td><td>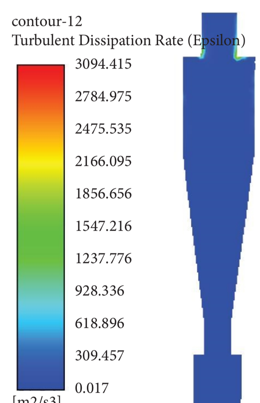
</td><td>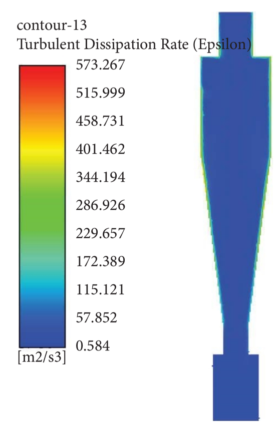
</td><td>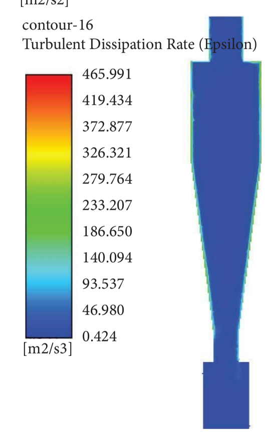
</td></tr>
</table>

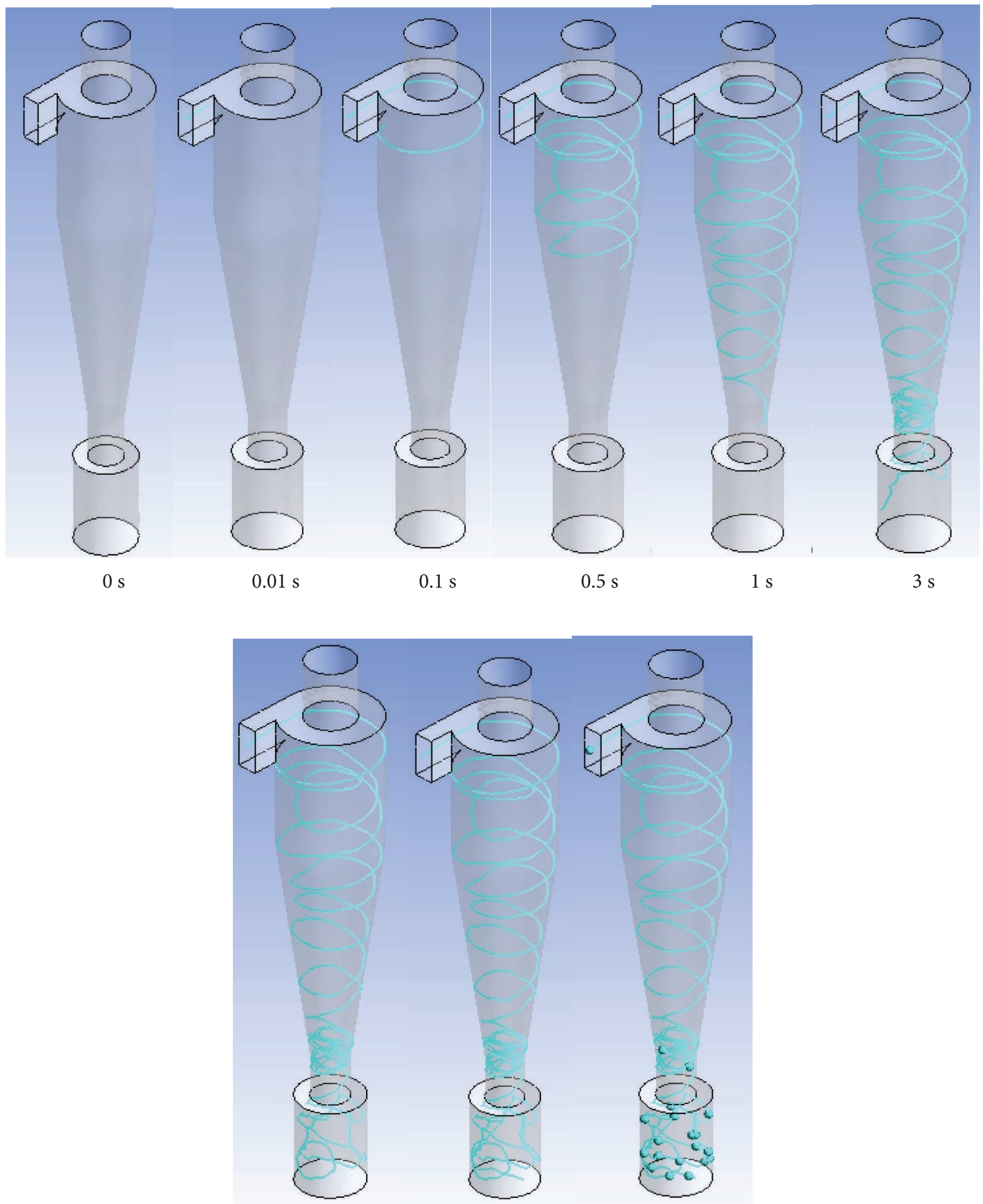

Figure 29: Trajectory of a particle inside the separator.

4. Conclusion and Perspectives

The aim of the present study is to numerically simulate the turbulent and three-dimensional aerodynamic multiphase flow inside conventional industrial cyclone dust collector with a single tangential inlet. The numerical simulation tool Fluent R19.2 was our means, thanks to its simple and attractive interface; it allowed us to go from the generation of the 3D schematic of the separator to the results, through the meshing and the implementation of the various simulation parameters. This software allowed us to obtain with clarity the phenomena that govern the turbulent flow inside the cyclone separator. Some of the results obtained are in good agreement with the experimental and numerical results.

The conclusions drawn from this work are as follows.

The mean velocity field is made up of three components, each with a very specific role in the turbulent flow inside the cyclone separator: the tangential velocity, which has the highest value, is responsible for separating the particles (discrete phase) from the gas that constitutes the continuous phase in the quasi-free outer vortex; then the axial velocity is responsible for transporting these particles toward the base of the collector in a helical fashion, still in the quasi-free vortex; and finally, the radial component is responsible to returning the flow with the finest particles, but this time in the quasi-forced inner vortex.

Efficiency and pressure drop are performance indicators that increase with inlet speed. The former is an advantage, but the latter a disadvantage; so it is up to the engineer to find the right balance between the energy resources available and the efficiency margin to be achieved. Efficiency also increases with particle size for given inlet velocity. But efficiency can also be varied for a given particle size by varying the inlet velocity.

Of the three numerical models used, the RSM model proved to be the most suitable for studying the turbulent flow inside the cyclone, but it is characterised by a very long calculation time and requires large machine resources. An alternative to this model is the RNG K-epsilon model, which offers a reasonable calculation time with acceptable results.

Analysis of the empirical and semiempirical models shows that they can be used to calculate efficiency and pressure drops. The Stairmand model correlates well with experimental data, probably because the geometry of the separator we have chosen is the high-efficiency Stairmand model. The Casal and Martine–Benet and Dirgo models can also be used. In terms of efficiency, the Iozia and Leith model proved to be the most suitable. The first pressure drops model correlate perfectly with the RNG K-epsilon numerical model, so it can be an alternative.

Finally, it should be said that the new generation of separators for which no results have been presented in this work, has a higher efficiency gap of between 3 and 12% for particle smaller than 10 μm and high pressure drops compared with the simple cyclone separator. This is due to the progressive friction experienced by the multiphase vortex flow between the channels inside the cyclone. The result is an increase in pressure drop and also an increase in efficiency. However, it should also be noted that this new generation of cyclone requires meticulous design in terms of the arrangement and orientation of the channels in the separation chamber (cylinder). Once again, it should be remembered that in order to choose the right type of separator for a specific application, it is up to the engineer to find the right balance between the energy resources available and the efficiency margin to be achieved.

Nomenclature

D: Body diameter, m
a: Inlet tube length, m
b: Inlet tube width, m
D_e: Vortex finder diameter, m
S: Vortex finder height, m
B_c: Cone base diameter, m
H: Cyclone height, m
h: Body height, m
L_e: External extension of the vortex finder, m
L_i: Extension of the inlet, m
H_t: Cone tip length, m
H_k: Collector height, m
D_k: Collector diameter, m
g: Gravitational acceleration, m/s^2
F_c: centrifugal $Force$, N
m: Mass, kg
V_c: centrifugal $velocity$, m/s
ω: Rotational velocity, rad/s
r: Radius, m
Δ_P: Pressure drop, pa
F_g: force of gravity, N
F_d: resisting forces, N
ρ: densities of the gas, kg/m^3
ρ_p: densities of the particle, kg/m^3
x_{pi}: The ith coordinate of the particle position, m
u_{pi}: The ith coordinate of the particle velocity, m/s
F_x: Saffman force, N
g_i: the acceleration due to gravity in i direction m/s^2
C_d: coefficient of resistance for spherical particles
τ_P: relaxation time of the particle, s
R_{ep}: Reynolds number
μ: Dynamic viscosity
d_p: Particle diameter, m
d_{ij}: Strain tensor
τ: Shear stress components (τ_{ij}^l)
P: Pressure, Pa
E: Energy, J

Subscripts

i, j, k, l: $i, j, k\ and\ l^{th}$ direction
p, x: particle

Abbreviations

RANS: Reynolds averaged Navier-Stokes
RSM: Reynolds stress model
RNG: Renormalization group
LES: Large eddy simulation
DNS: Direct numerical simulation.

Data Availability

The data used to support the findings of this study are included within the article.

Conflicts of Interest

The authors declare that they have no conflicts of interest that could have appeared to influence the work reported in this paper.

Authors' Contributions

Paganel Vermande Tchinda conceptualized the study, proposed the methodology, provided the software, wrote the original draft, and contributed to visualization. Dr. Epee Fabrice Alban conceptualized the study and wrote, reviewed, and edited the article. Dr. Cyrille Mezoue Adiang conceptualized the study, wrote, reviewed, and edited the article, and performed supervision. Pr. Claude Valery Ngayihi Abbe conceptualized the study, wrote, reviewed, and edited the article, performed supervision, and provided project administration.

Acknowledgments

This work was fully founded by the University of Douala.

References

[1] X. Simon, "Study of pneumatic unclogging of baghouse dust collectors," in *Process and Product Engineering*, National institute for research and security, Bengaluru, India, 2005.

[2] Z. Ilhem, "Simulation Numérique En Régime Turbulent De L'influence Du Débit et du Champ Thermique sur le Comportement du Vortex d'un Cyclone," in *Departement de Génie Mécanique 2008*, Université Mentouri Constantine, Algeria, North Africa, 2023.

[3] O. R. Nassaj, D. Toghraie, and M. Afrand, "Effects of multi inlet guide channels on the performance of a cyclone separator," *Powder Technology*, vol. 356, pp. 353–372, 2019.

[4] A. C. Hoffmann and L. E. Stein, *Gas Cyclones and Swirl Tubes: Principles, Design and Operation*, Springer-Verlag, Berlin, Germany, 2008.

[5] C. Cortes and A. Gil, "Modeling the gas and particle flow inside cyclone separators," *Progress in Energy and Combustion Science*, vol. 33, no. 5, pp. 409–452, 2007.

[6] B. Martin, *design de séparateurs cycloniques, 6GIN333 projet de conception en ingénierie. 24 août 2011*, Université du Québec à Chicoutimi, Saguenay, Canada.

[7] K. Nabil, *Study of Aerodynamics and Particle Filtration in a Cyclone Separator in Mechanical Engeneering Department*, University of Mentouri Constantine, Constantine, Algérie, 2015.

[8] E. Dehdarinejad and M. Bayareh, "An overview of numerical simulations on gas-solid cyclone Separators with tangential inlet," *ChemBioEng Reviews*, vol. 8, no. 4, pp. 375–391, 2021.

[9] S. G. Bogodage and A. Y. T. Leung, "CFD simulation of cyclone separators to reduce air pollution," *Powder Technology*, vol. 286, pp. 448–506, 2015.

[10] K. Talbi, I. Zeghbid, A. Donnot, and Z. Nemouchi, "Simulation numérique en régime turbulent de l'influence du débit et du champ thermique dans un cyclone," *Journal of Renewable Energies*, vol. 14, no. 3, pp. 501–515, 2023.

[11] S. Wang, H. Li, R. Wang, X. Wang, R. Tian, and Q. Sun, "Effect of the inlet angle on the performance of a cyclone separator using CFD-DEM," *Advanced Powder Technology*, vol. 2137, pp. 1–13, 2018.

[12] R. Utikar, N. Darmawan, M. Tade et al., *Hydrodynamic Simulation of Cyclone Separators Computational Fluid Dynamics Book*, IntechOpen Limited, London, UK, 2010.

[13] P. B. Fu, F. Wang, X. J. Yang, L. Ma, X. Cui, and H. L. Wang, "Inlet particle-Sorting cyclone for the Enhancement of PM2.5 separation," *Environmental Science and Technology*, vol. 51, no. 3, pp. 1587–1594, 2017.

[14] A. Avci and I. Karagoz, "Effects of flow and geometrical parameters on the collection efficiency in cyclone separators," *Journal of Aerosol Science*, vol. 34, no. 7, pp. 937–955, 2003.

[15] K. S. Lim, H. Kim, and K. W. Lee, "Comparative performances of conventional cyclones and a double cyclone with and without an electric field," *Journal of Aerosol Science*, vol. 35, no. 1, pp. 103–116, 2004.

[16] A. Raoufi, M. Shams, M. Farzaneh, and R. Ebrahimi, "Numerical simulation and optimization of fluid flow in cyclone vortex finder," *Chemical Engineering and Processing: Process Intensification*, vol. 47, no. 1, pp. 128–137, 2008.

[17] K. Elsayed and C. Lacor, "The effect of cyclone inlet dimensions on the flow pattern and performance," *Applied Mathematical Modelling*, vol. 35, no. 4, pp. 1952–1968, 2011.

[18] L. S. Brar, R. P. Sharma, and R. Dwivedi, "Effect of vortex finder diameter on flow field and collection efficiency of cyclone separators," *Particulate Science and Technology*, vol. 33, no. 1, pp. 34–40, 2015.

[19] K. S. Lim, S. B. Kwon, K. Lee, and K. W. Lee, "Characteristics of the collection efficiency for a double inlet cyclone with clean air," *Journal of Aerosol Science*, vol. 34, no. 8, pp. 1085–1095, 2003.

[20] B. Zhao, H. Shen, and Y. Kang, "Development of a symmetrical spiral inlet to improve cyclone separator performance," *Powder Technology*, vol. 145, no. 1, pp. 47–50, 2004.

[21] E. Dehdarinejad, M. Bayareh, and M. Ashrafizaadeh, "Impact of cone wall roughness on turbulence swirling flow in a cyclone separator," *Chemical Papers*, vol. 76, no. 9, pp. 5579–5599, 2022.

[22] J. X. Yang, G. G. Sun, and C. Z. Gao, "Effect of the inlet dimensions on the maximum-efficiency cyclone height," *Separation and Purification Technology*, vol. 105, pp. 15–23, 2013.

[23] S. Bernardo, M. Mori, A. P. Peres, and R. P. Dionisio, "3-D computational fluid dynamics for gas and gas-particle flows in a cyclone with different inlet section angles," *Powder Technology*, vol. 162, no. 3, pp. 190–200, 2006.

[24] D. Misiulia, A. G. Andersson, and T. S. Lundstrom, "Effects of the inlet angle on the collection efficiency of a cyclone with helical-roof inlet," *Powder Technology*, vol. 305, pp. 48–55, 2017.

[25] T. Dzuibak, "Experimental investigation of possibilities to improve filtration efficiency of tangential inlet return cyclone by modification of design," *Energies*, vol. 15, 37 pages, 2022.

[26] W. P. Martignoni, S. Bernardo, and C. L. Quintani, "Evaluation of cyclone geometry and its influence on performance parameters by computational fluid dynamics (CFD)," *Brazilian Journal of Chemical Engineering*, vol. 24, no. 1, pp. 83–94, 2007.

[27] J. Gimbun, T. Chuah, T. S. Choong, A. Fakhru'l-Razi, and A. Fakhru'l-Razi, "Prediction of the effects of cone tip diameter on the cyclone performance," *Journal of Aerosol Science*, vol. 36, no. 8, pp. 1056–1065, 2005.

[28] T. G. Chuah, J. Gimbun, and T. S. Choong, "A CFD study of the effect of cone dimensions on sampling aerocyclones performance and hydrodynamics," *Powder Technology*, vol. 162, no. 2, pp. 126–132, 2006.

[29] R. B. Xiang and K. W. Lee, "Numerical study of flow field in cyclones of different height," *Chemical Engineering and Processing: Process Intensification*, vol. 44, no. 8, pp. 877–883, 2005.

[30] H. Yoshida, Y. Hayase, K. Fukui, and T. Yamamoto, "Effect of conical length on separation performance of sub-micron particles by electrical hydro-cyclone," *Powder Technology*, vol. 219, pp. 29–36, 2012.

[31] O. Hamdy, M. A. Bassily, H. M. El-Batsh, and T. A. Mekhail, "Numerical study of the effect of changing the cyclone cone length on the gas flow field," *Applied Mathematical Modelling*, vol. 46, pp. 81–97, 2017.

[32] Z.-W. Zhang, Q. Li, and Y.-H. Zhang, "Simulation and experimental study of effect of vortex finder structural parameters on cyclone separator performance," *Separation and Purification Technology*, vol. 226, 2022.

[33] E. Yohana, M. Tauviqirrahman, D. A. Laksono, H. Charles, K. H. Choi, and M. E. Yulianto, "Innovation of vortex finder geometry (tapered in-cylinder out) and additional cooling of body cyclone on velocity flow field, performance, and heat transfer of cyclone separator," *Powder Technology*, vol. 399, Article ID 117235, 2022.

[34] J. Kim and K. Lee, "Experimental study of particle collection by small cyclones," *Aerosol Science and Technology*, vol. 12, no. 4, pp. 1003–1015, 1990.
[35] A. Ogawa, A. Hironaka, T. Kato, and O. Seito, "Velocity distributions of gas flow and the separation efficiency of the semispherical cyclone," *Advanced Powder Technology*, vol. 2, no. 3, pp. 191–212, 1991.
[36] J. Jiao, Y. Zheng, J. Wang, and G. Sun, "Experimental and numerical investigations of a dynamic cyclone with a rotary impeller," *Chemical Engineering and Processing: Process Intensification*, vol. 47, no. 9-10, pp. 1861–1866, 2008.
[37] A. Raoufi, M. Shams, and H. Kanani, "CFD analysis of flow field in square cyclones," *Powder Technology*, vol. 191, no. 3, pp. 349–357, 2009.
[38] W. Wang, P. Zhang, L. Wang, G. Chen, J. Li, and X. Li, "Structure and performance of the circumfluent cyclone," *Powder Technology*, vol. 200, no. 3, pp. 158–163, 2010.
[39] A. Chlebnikovas, A. Kilikevičius, J. Selech et al., "The numerical modeling of gas movement in a single inlet new generation multi-channel cyclone separator," *Energies*, vol. 14, no. 23, p. 8092, 2021.
[40] P. Baltrėnas, P. Vaitiekūnas, I. Jakštonienė, and K. Simona, "Study of gas–solid flow in a multichannel cyclone/oro ir kietųjų dalelių srauto daugiakanaliame ciklone tyrimas," *Journal of Environmental Engineering and Landscape Management*, vol. 20, no. 2, pp. 129–137, 2012.
[41] A. Chlebnikovas and P. Baltrenas, "Research and analysis of Aggressive conditions formation into a multi channel cyclone," *Energy Procedia*, vol. 113, pp. 69–76, 2017.
[42] A. Chlebnikovas and R. Jasevicius, "Investigation of the interaction of particulate matter and its separation from the gas flow in a multi-channel cyclone with recirculation," *Granular Matter*, vol. 24, no. 4, p. 98, 2022.
[43] B. Pranas, C. Andreas, L. Therese, and C. Aleksandras, "Investigation on particulate matter and gas motion processes in the advanced multi-channel cyclone-separator with secondary gas inlets," *Environemental Engineering Research*, vol. 27, no. 1, pp. 1–13, 2022.
[44] D. Misiulia, S. Antonyuk, A. G. Andersson, and T. S. Lundström, "High-efficiency industrial cyclone separator: a CFD study," *Powder Technology*, vol. 364, pp. 943–953, 2020.
[45] I. Karagoz, A. Avci, A. Surmen, and O. Sendogan, "Design and performance evaluation of a new cyclone separator," *Journal of Aerosol Science*, vol. 59, pp. 57–64, 2013.
[46] S. Dong, Y. Jiang, R. Jin, K. Dong, and B. Wang, "Numerical study of vortex eccentricity in a gas cyclone," *Applied Mathematical Modelling*, vol. 80, pp. 683–701, 2020.
[47] S. Fu, F. Zhou, G. Sun, H. Yuan, and J. Zhu, "Performance evaluation of industrial large-scale cyclone separator with novel vortex finder," *Advanced Powder Technology*, vol. 32, no. 3, pp. 931–939, 2021.
[48] S. Venkatesh, S. P. Sivapirakasam, M. Sakthivel, S. Ganeshkumar, M. Mahendhira Prabhu, and M. Naveenkumar, "Experimental and numerical investigation in the series arrangement square cyclone separator," *Powder Technology*, vol. 383, pp. 93–103, 2021.
[49] K. Elsayed and C. Lacor, "Optimization of the cyclone separator geometry for minimum pressure drop using mathematical models and CFD simulations," *Chemical Engineering Science*, vol. 65, no. 22, pp. 6048–6058, 2010.
[50] I. M. B. M De Silva, *Reverse Flow Cyclone for Collection of tea Dust*, university of Moratuwa Sri Lanka, Moratuwa, Sri Lanka, 2003.
[51] C. J. Stairmand, "Pressure drops in cyclone separators," *Industrial and Engineering Chemistry*, vol. 16, no. B, pp. 409–411, 1949.
[52] M. Slack, *Cyclonic Separator*, Fluent Europe Ltd, New York, NY, USA, 2002.
[53] H. Versteeg and W. Malalasekera, *Introduction to Computational Fluid Dynamics, the Finite Volume Method*, Prentice-Hall, New York, NJ, USA, 1995.
[54] G. Dominique, *Modélisation et simulation de la turbulence compressible dans les écoulements cisaillés supersoniques*, Université de la Méditerranée, Marseille, France, 1997.
[55] A. N. Kolmogorov, "Equations of turbulent motion of an incompressible turbulent fluid," *Izvestiya Akademii Nauk SSR, Seriya Fizicheskaya*, vol. 4, pp. 1-2, 1942.
[56] Ansys, "Solver modeling Documentation," 2017, https://docs.itascacg.com/3dec700/common/kernel/doc/manual/model/commands/cmd_model.solve.html.
[57] K. Elsayed and C. Lacor, "Investigation of the geometrical parameters effects on the performance and the flow-field of cyclone separators using mathematical models and large eddy simulation," in *Proceedings of the 13th International Conference on Aerospace sciences and aviation technology, ASAT-13*, Cairo, Egypt, May 2009.
[58] K. Elsayed and C. Lacor, "The effect of the dust outlet geometry on the performance and hydrodynamics of gas cyclones," *Computers and Fluids*, vol. 68, pp. 134–147, 2012.
[59] D. Park, J. Cha, M. Kin, and J. S. Go, "Multi-objective optimization and comparison of surrogate models for separation performances of cyclone separator based on CFD, RSM, GMDHneural network, back propagation-ANN and genetic algorithm," *Engineering Applications of Computational Fluid Mechanics*, vol. 236, pp. 37–46, 2019.
[60] W. Lingjuan, "Theoretical study of cyclone design," in *Biological and Agricultural Engineering*, Texas A&M University, New York, TX, USA, 2004.
[61] Ansys, "Solver theory Documentation," 2017, https://www.afs.enea.it/project/neptunius/docs/fluent/html/th/node359.htm.
[62] A. Kępa, "Division of outlet flow in a cyclone vortex finder—the CFD calculations," *Separation and Purification Technology*, vol. 75, no. 2, pp. 127–131, 2010.
[63] G. Wan, G. Sun, X. Xue, and M. Shi, "Solids concentration simulation of different size particles in a cyclone separator," *Powder Technology*, vol. 183, no. 1, pp. 94–104, 2008.
[64] Y. Qiu, B. Deng, and C. N. Kim, "Numerical study of the flow field and separation efficiency of a divergent cyclone," *Powder Technology*, vol. 217, pp. 231–237, 2012.
[65] L. Ma, D. B. Ingham, and X. Wen, "Numerical modelling of the fluid and particle penetration through small sampling cyclones," *Journal of Aerosol Science*, vol. 31, no. 9, pp. 1097–1119, 2000.
[66] W. Griffiths and F. Boysan, "Computational fluid dynamics (CFD) and empirical modelling of the performance of a number of cyclone samplers," *Journal of Aerosol Science*, vol. 27, no. 2, pp. 281–304, 1996.
[67] H. Yoshida, Y. Kwan-Sik, K. Fukui, S. Akiyama, and S. Taniguchi, "Effect of apex cone height on particle classification performance of a cyclone separator," *Advanced Powder Technology*, vol. 14, no. 3, pp. 263–278, 2003.
[68] T. Chuah, J. Gimbun, T. S. Choong, and Y. Choong, "A CFD study of the effect of cone dimensions on sampling aerocyclones performance and hydrodynamics," *Powder Technology*, vol. 162, no. 2, pp. 126–132, 2006.
[69] K. U. Bhaskar, Y. R. Murthy, M. R. Raju, S. Tiwari, J. K. Srivastava, and N. Ramakrishnan, "CFD simulation and

experimental validation studies on hydrocyclone," *Minerals Engineering*, vol. 20, no. 1, pp. 60–71, 2007.

[70] K. Elsayed and C. Lacor, "Numerical modeling of the flow field and performance in cyclones of different cone-tip diameters," *Computers and Fluids*, vol. 51, no. 1, pp. 48–59, 2011.

[71] S. K. Shukla, P. Shukla, and P. Ghosh, "Evaluation of numerical schemes for dispersed phase modeling of cyclone separators," *Engineering Applications of Computational Fluid Mechanics*, vol. 5, no. 2, pp. 235–246, 2011.

[72] F. J. de Souza, R. de Vasconcelos Salvo, and D. A. de Moro Martins, "Large eddy simulation of the gas–particle flow in cyclone separators," *Separation and Purification Technology*, vol. 94, pp. 61–70, 2012.

[73] M. Bohnet, "Influence of the gas temperature on the separation efficiency of aerocyclones," *Chemical Engineering and Processing: Process Intensification*, vol. 34, no. 3, pp. 151–156, 1995.

[74] K. S. Lim, K. W. Lee, and M. R. Kuhlman, "An experimental study of the performance factors affecting particle collection efficiency of the electrocyclone," *Aerosol Science and Technology*, vol. 35, no. 6, pp. 969–977, 2001.

[75] H. Yoshida, K. Fukui, K. Yoshida, and E. Shinoda, "Particle separation by Iinoya's type gas cyclone," *Powder Technology*, vol. 118, no. 1-2, pp. 16–23, 2001.

[76] S. Demir, A. Karadeniz, and M. Aksel, "A practical model for estimating pressure drop in cyclone separators: an experimental study," *Powder Technology*, vol. 268, pp. 329–338, 2014.

[77] J. Casal and J. M. Martinez-Benet, "A better way to calculate cyclone pressure drop," *Chemical Engineering*, vol. 99, pp. 100–111, 1983.

[78] A. K. Coker, "Understand cyclone design," *Chemical Engineering Progress*, vol. 89, pp. 51–55, 1993.

[79] J. Dirgo, *Relationships between Cyclone Dimensions and Performance*, Harvard University, Cambridge, CA, USA, 1988.

[80] C. B. Shepherd and C. E. Lapple, "Air pollution control: a design approach," in *Cyclones*, pp. 127–129, Woveland Press Inc, Long Grove, IL, USA, 1939.

[81] J. Gimbun, T. G. Chuah, A. Fakhru'l-Razi, and T. S. Choong, "The influence of temperature and inlet velocity on cyclone pressure drop: a CFD study," *Chemical Engineering and Processing: Process Intensification*, vol. 44, no. 1, pp. 7–12, 2005.

[82] D. L. Iozia and D. Leith, "The logistic function and cyclone Fractional efficiency," *Aerosol Science and Technology*, vol. 12, no. 3, pp. 598–606, 1990.

[83] R. Sardara, J. Oha, M. Kima, J.-E. Leeb, S. Kima, and K. Chun, "The effect of inlet velocity, gas temperature and particle size on the performance of double cyclone separator," *Chemical Engineering and Processing- Process Intensifcation*, vol. 191, pp. 1–12, 2023.

[84] J. Gimbun, S. Y. Thomas, and A. Fakhru'l-Razi, "Prediction of the effect of dimension, particle density, temperature, and inlet velocity on cyclone collection efficiency," *Journal of Technology*, vol. 40, pp. 37–50, 2004.

[85] Z. Chen, Y. Tian, and Q. Zhuang, "Effect of gas flow rate on separation efficiency at different scaling scales of cyclone separators," *Frontiers in Heat and Mass Transfer*, vol. 20, no. 26, pp. 1–11, 2023.

[86] D. K. Le and J. Y. Yoon, "Numerical investigation on the performance and flow pattern of two novel innovative designs of cyclone separator four-inlet," *Chemical Engineering and Processing: Process Intensification*, vol. 150, pp. 1–12, 2020.

[87] E. Dehdarinejad and M. Bayareh, "Impact of non-uniform surface roughness on the erosion rate and performance of a cyclone separator," *Chemical Engineering Science*, vol. 249, Article ID 117351, 2022.

[88] P. Zhang, J. Duan, G. Chen, and W. Wang, "Numerical investigation on gas-solid flow in a circumfluent cyclone separator," *Aerosol and Air Quality Research*, vol. 19, no. 5, pp. 971–980, 2019.

[89] T. Frank, E. Wassen, and Q. Yu, "Lagrangian prediction of disperse gas particle flow in cyclone separators," in *Proceedings of the Third International Conference on Multiphase Flow*, The Hague, Netherlands, May 1998.

[90] M. Morin, L. Raynal, S. R. Karri, R. Cocco, and G. Ahmadi, "Effect of solid loading and inlet aspect ratio on cyclone efficiency and pressure drop: experimental study and CFD simulations," *Powder Technology*, vol. 377, pp. 174–185, 2021.

[91] C. Fredriksson, *Exploratory Experimental and Theoretical Studies of Cyclone Gasification of wood Powder*, Lulea University of Technology, Luleå, Sweden, 1999.

[92] J. Gimbun, T. G. Chuah, T. S. Y. Choong, and A. Fakhru'l-Razi, "A CFD study on the prediction of cyclone collection efficiency," *International Journal for Computational Methods in Engineering Science and Mechanics*, vol. 6, no. 3, pp. 161–168, 2005.